Current Opinion in Solid State & Materials Science xxx (xxxx) xxxx

Contents lists available at ScienceDirect

Current Opinion in Solid State & Materials Science

journal homepage: www.elsevier.com/locate/cossms

Mechanics at the interfaces of 2D materials: Challenges and opportunities

Zhaohe Dai, Nanshu Lu, Kenneth M. Liechti, Rui Huang*

Department of Aerospace Engineering and Engineering Mechanics, University of Texas, Austin, TX 78712, United States

A B S T R A C T

At the interfaces of 2D materials, the solid-state condensed matter physics is closely intertwined with the mechanics in terms of adhesion/separation and friction as well as deformation of 2D materials. With atomically thin 2D layers in atomically close proximity, the chemical, physical, and mechanical interactions simultaneously evolve and influence each other, leading to a wide range of topological structures and properties across nano- and micro-scales. Can the study on the mechanics of interfaces help to understand the physics and chemistry at the interfaces of 2D materials or vice versa? This Opinion aims to highlight the recent mechanics research on such material interfaces, where a multiscale, multidisciplinary effort is most effective moving forward with plenty of challenges and opportunities.

1. Introduction

Two-dimensional (2D) materials are a relatively new class of thin materials consisting of a single layer or a few layers of covalently bonded atoms, including graphene, hexagonal boron-nitride (hBN), and transition metal-dichalcogenides (TMDs, e.g., MoS_2 and WSe_2). Over the last decade, there has been an enormous surge of interest in the unusual, and technologically useful, properties of the 2D materials. More recently, a new paradigm for material design has emerged by stacking different 2D materials on top of one another [1–3]. The resulting layered structures, often called van der Waals (vdW) heterostructures, feature strong intralayer covalent bonds and relatively weak interlayer vdW interactions. These highly anisotropic interactions provide vdW layered structures with tunable collective properties via the vertical stacking sequence and the relative twisting or straining between the layers [4–11]. Furthermore, a plethora of opportunities could be opened by applying mechanical loads to such structures, including bending, stretching, twisting, and hydrostatic pressure [8,12–14]. Such an unprecedented level of tunability has led to several observations of new phenomena (e.g., 'magic-angle' superconductivity [5] and pseudomagnetic fields [12]) and propelled these vdW materials into a wide range of technological applications (e.g. phototransistors, light-emitting diodes, etc.) [1–3]. In order to fulfill the promising applications of the 2D materials and their heterostructures, it is critically important to understand the mechanics at the interfaces of various 2D materials, where the solid-state condensed matter physics is closely intertwined with the mechanics in terms of adhesion/separation and friction as well as deformation of 2D materials [15–18].

In this Opinion, we review recent research on the mechanics of 2D material interfaces. Our primary focus is on the recent theoretical and experimental advances towards the understanding of the normal and tangential interactions at the interfaces of 2D materials, including 2D-3D interfaces between 2D materials and 3D bulk substrates (Section 2) and 2D-2D interfaces between various 2D materials (Section 3). These discussions aim to highlight how the physical, chemical, and mechanical interactions simultaneously evolve and influence one another at 2D material interfaces, and how such interweaving leads to a wide range of topological structures and properties. The multiscale and multidisciplinary nature of the interfaces offers both grand challenges and ample opportunities for future research.

2. 2D-3D interfaces

2.1. Normal interactions: Adhesion and separation

Interactions in the normal direction of an interface are often described as adhesion or adhesive interactions. As an atomically thin 2D material approaches to or separates from the surface of a 3D substrate, it experiences a normal traction (σ) that depends on the normal distance (δ_n) between the 2D material and the surface (Fig. 1A). The interfacial potential energy (Φ_n) is minimized at an equilibrium separation ($\delta_n = \delta_0$) with zero traction and vanishes when the 2D material is fully separated from the substrate ($\delta_n \to \infty$). The adhesion energy (Γ_0) is then defined as the change of the interfacial potential energy (per unit area) between the equilibrium state ($\delta_n = \delta_0$) and the separated state ($\delta_n \to \infty$), also called work of adhesion or work of separation depending on the processes related to either approach or separation. Ideally, if these processes are thermodynamically reversible, the works of adhesion and separation would be identical. However, in practice, the two are often different, known as adhesion hysteresis, suggesting energy dissipation and irreversible mechanisms (e.g., snapping) during the approach/separation processes. To measure the adhesion energy of 2D

* Corresponding author.
E-mail address: ruihuang@mail.utexas.edu (R. Huang).

https://doi.org/10.1016/j.cossms.2020.100837
Received 16 March 2020; Received in revised form 1 July 2020; Accepted 8 July 2020

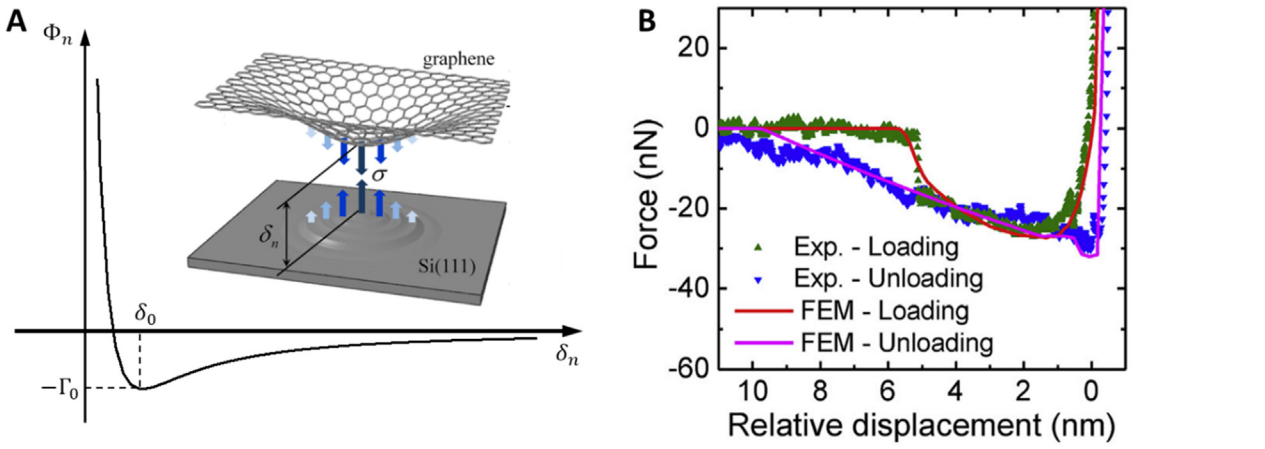

Fig. 1. (**A**) Schematic of the interaction potential energy between graphene and a 3D substrate. Inset is adopted with permission from [19]. (**B**) Measured loading–unloading force profiles from displacement-controlled nanoindentation with a diamond tip indenting monolayer graphene on silicon oxide in a dry nitrogen environment. Figure is adapted with permission from [20].

Table 1
Measurements of 2D-3D interfacial adhesion/separation energies (G for graphene, A and S denote adhesion and separation, respectively).

Interface	Adhesion Energy (mJ/m^2)	Method	Ref
G–SiO_2	93 ± 1 (A)	Spontaneous bubbles	[30]
	567.14 (A)	Nanoparticle	[33]
	276–453 (A)	Nanoparticle	[34]
	310–450 (S)	Pressurized blisters	[21]
	460 ± 23 (S)	Nanoindentation	[31]
	580 ± 20 (S)	Nanoindentation	[32]
G-Si	151 ± 28 (A)	Nanoparticle	[24]
	357 ± 16 (S)	DCB	[19]
G–Cu	210–510 (S)	Pressurized blisters	[22,35,36]
	720 ± 70 (S)	DCB	[23]
	750 ± 38 (S)	Nanoindentation	[31]
G-Cu (foil)	740–1530 (S)	Pressurized blister	[37]
	6000 (S)	DCB	[38]
G–Pt	4021(A)	Nanoparticle	[33]
G–Au	7687(A)		
G–CaF_2	104 (A)	Spontaneous bubbles	[30]
G-Ice	124 ± 30 (A)		
G-Epoxy	3400 (S)	DCB	[38]
G–PMMA	2.8–84.4 (S)	Buckle delamination	[27]
G-Glass	~10–140 (S)	Peeling	[39]
MoS_2–PDMS	18 ± 2 (S)	Buckle delamination	[26]
MoS_2–Al_2O_3	101 ± 15 (A)	Spontaneous bubbles	[30]
MoS_2–SiO_2	82 ± 1 (A)	Spontaneous bubbles	[30]
	482.48 (A)	Nanoparticle	[33]
	170 ± 33 (S)	Buckle delamination	[28]
MoS_2–SiO_x	42 ± 20 (A)	Pressurized blisters	[40]
	220 ± 35 (S)		
MoS_2–Si_3N_4	429 (A)	Nanoparticle	[33]
	252 ± 41 (S)	Buckle delamination	[28]
MoS_2–Pt	690 (A)	Nanoparticle	[33]
MoS_2–Au	1207 (A)		

materials to 3D substrates, several experimental methods have been developed, such as pressurized blister tests [21,22], double cantilever beam (DCB) tests [19,23], nanoparticle intercalation [24,25], buckle-delamination [26–29], spontaneous nanobubbles [30], and nanoindentation [20,31,32]. Strictly speaking, the measurements by the tests involving pressurized blisters, DCB and buckle-delamination typically measure the work of separation, while nanoparticle intercalation and spontaneous nanobubbles yield the work of adhesion. Adhesion hysteresis is commonly observable in nanoindentation experiments with loading and unloading cycles (Fig. 1B). Table 1 summarizes the reported measurements of the adhesion/separation energies between various 2D materials and 3D substrates.

In addition to the adhesion energy, further insights into the underlying mechanisms of the interactions at the 2D-3D interfaces can be gained from the traction-separation relations (TSRs) associated with approach or separation. For example, the same adhesion energy may result from completely different mechanisms with very different adhesive strengths (maximum traction) and different ranges of interactions. However, compared to the adhesion energy measurements, it is generally more challenging to measure the interfacial TSRs, especially for 2D materials because of the ultrathin membrane structure. Na et al. [19] extracted TSRs for the interactions between wet-transferred, CVD grown graphene and a silicon substrate from DCB experiments. Although the measured adhesion energy is commensurate with vdW interactions, the deduced TSRs extended to a much longer range (>100 nm) than those normally associated with vdW forces, suggesting that interaction mechanisms other than vdW forces should be considered. Suk et al. [20] conducted displacement-controlled nanoindentation experiments on graphene, based on which the TSRs were extracted for interactions between the diamond tip and graphene as well as between graphene and the silicon oxide substrate. The TSRs exhibited the characteristics of capillary forces with long tails in addition to the vdW forces at shorter ranges, despite the fact that the experiments were conducted in a dry nitrogen environment.

Theoretically, adhesive interactions between a 2D material and its 3D substrate are often attributed to the ubiquitous vdW forces, without specific chemical bonds. Typical values of adhesion energy due to vdW forces are on the order of 100 mJ/m^2, while the interaction strengths can be up to 200 MPa and the range is limited to nanoscale (<10 nm), as predicted by density functional theory (DFT) calculations [41]. However, adhesive interactions over longer ranges have been observed, for example, in the island blister test [42], where a structural pull-in instability may be triggered by minute vdW forces over the long tail in the associated TSR [43]. Moreover, there are growing experimental evidences that suggest that other interaction mechanisms could be active: (1) A wide range of values have been reported for the adhesion energy of 2D materials (Table 1), from ~3 to ~7000 mJ/m^2; (2) The TSRs extracted from experiments had much lower strengths but longer ranges compared to those predicted for vdW interactions [19,20]; (3) The values of adhesion energy, strength, and range of the interactions were found to be dependent on the loading conditions such as the mode-mix [35,36] and loading rate [38,44].

Theoretical understanding on the underlying mechanisms of the 2D-3D interactions beyond vdW forces remains limited. Among others, the effect of water was considered for wet adhesion of graphene [45], which could extend the interaction range by capillary bridging, but the

adhesion energy remained low. Discrete, short-range interactions due to reactive defects on the surface of silicon oxide were also suggested as a potential cause for the ultra-strong adhesion of graphene [46]. Clearly, the interfacial chemistry (e.g., water molecules, bonding types and density) could be important to understand the adhesive interactions [27,39,45]. Higher adhesion energy could also result from mixed-mode conditions with coupled normal and shear interactions, as a well-known toughening mechanism related to asperity locking of rough surfaces [35,36]. Indeed, the effective adhesion energy of graphene was found to depend on the surface roughness [47], with apparently higher adhesion energy for monolayer graphene than few-layered graphene [21,48]. The adhesive interactions between an ultrathin 2D material and a rough surface of a 3D substrate could lead to conformal, partly conformal or non-conformal morphology, depending on the bending rigidity of the 2D material and the roughness characteristics [47]. Interestingly, the adhesive interactions between CVD graphene and its seed copper foil were found to be particularly strong, with a separation energy of ~6000 mJ/m^2 [38], much larger than expected from typical vdW forces. The CVD graphene conformed to the copper surface and formed regular ridges. The root-mean-square (RMS) roughness was about 10 nm within each copper grain, but increased to about 800 nm at millimeter scales. More recent measurements from blister tests [37,49] have shown that the graphene/seed copper interfacial toughness increased with increasing roughness. In contrast, for thin copper films deposited on silicon, the surface roughness was much smaller and so was the adhesion energy of graphene grown on such copper films [23,50,51]. Thus, the effects of surface roughness and its scale dependence could be important for quantitative understanding of the 2D-3D adhesive interactions.

The rate effect on adhesion has facilitated the selective transfer of graphene from a seed copper foil [38]. However, the underlying mechanism is not well understood. One hypothesis is related to an interphase region that develops in the epoxy or other materials close to the graphene, where inelastic and rate-dependent deformation processes may occur. Alternatively, a thermally activated separation process could be at play, which would lead to both rate and temperature dependence of adhesion [52–54]. A recent study [44] suggested rate-dependent decohesion modes in graphene sandwiched interfaces, where the apparently rate-dependent adhesion energy was attributed to the deformation and damage of graphene during separation of the interfaces.

Moreover, how do the 2D-3D adhesive interactions depend on temperature? For monolayer graphene and other 2D materials, thermal rippling is inevitable at a finite temperature [55,56]. When supported on a substrate, although the adhesive interactions could considerably reduce thermal rippling, the presence of stochastic thermal rippling leads to an entropic repulsion. As a result, the effective adhesion energy would decrease with increasing temperature, as predicted by a statistical mechanics analysis and molecular dynamics (MD) simulations [57,58]. Alternatively, temperature-dependent traction-separation relations were also predicted by a thermally activated kinetic bond rupture model [54], offering another potential mechanism for the temperature dependence. However, to the best of our knowledge, temperature-dependent adhesion of 2D materials has not been observed experimentally.

Different interfacial chemistries have been exploited for the effective control of graphene-substrate adhesion. For example, Miskin et al. [39] measured the work of separation between graphene and a glass substrate whose surface was modified with monolayers of pyrene butyrate and acetate groups. They found that the work of separation depended on the density of pyrene groups, ranging between ~10 mJ/m^2 for an unmodified glass and a maximum value of ~140 mJ/m^2 (with 40 mol % pyrene butyrate). By peeling and re-adhesion, they observed a significant, rate-independent adhesion hysteresis. Dai et al. [27] used the buckle-delamination method to study adhesion of pristine graphene and oxygen-functionalized graphene to a PMMA substrate. They reported a much higher adhesion energy (~84.4 mJ/m^2) for the functionalized graphene than the pristine graphene (~2.8 mJ/m^2). These works have demonstrated the possibility of tunable adhesive interactions at the 2D-3D interfaces.

2.2. Friction and shear interactions

Interactions in the tangential direction of an interface can be described as friction or shear interactions, where shear tractions are transmitted as a result of relative sliding in terms of displacement or velocity or both. Two types of experiments have been conducted to investigate the friction and shear interactions between 2D materials and 3D objects. First, lateral force measurements using atomic force microscopy (AFM), also called friction force microscopy (FFM), have been conducted to characterize single nano-asperity sliding friction on surfaces coated with monolayer or few-layered 2D materials [59–63]. Second, shear interactions between 2D materials and their substrates have been examined by inducing relative sliding via stretching of the substrates [64–68], pulling 2D materials [69], and pressurized microblisters [70,71]. Moreover, interlayer friction and shear interactions between various 2D materials have also been studied extensively and are discussed in Section 3 as part of the 2D-2D interactions.

The FFM measures the lateral force as a nanoscale AFM tip slides on a surface in contact mode, typically with a constant normal force applied. Filleter et al. [59] observed atomic stick–slip friction by FFM on both monolayer and bilayer graphene grown epitaxially on SiC. Compared to the friction on bare SiC (with a carbon-rich surface), the average lateral force was reduced by an order of magnitude on a monolayer graphene and further reduced by a factor of 2 on a bilayer graphene. They suggested that the friction contrast arose from a dramatic difference in the electron–phonon coupling, with evidence from angle-resolved photoemission spectroscopy. Lee et al. [60] compared the frictional characteristics of graphene, MoS_2, $NbSe_2$, and hBN, exfoliated onto a silicon oxide substrate, to their bulk counterparts. Their FFM measurements revealed that friction monotonically decreased as the number of layers increased for all four materials (Fig. 2B), while the trend was suppressed for the 2D materials on an atomically flat mica surface. Both graphene and MoS_2 exhibited atomic stick–slip friction, with an unusual “strengthening” effect (Fig. 2A). While the absolute value of the measured friction force depends on many factors, including tip size, shape and composition, applied normal load, environment, and scan speed, the trend of decreasing friction with increasing thickness was found to be robust over a wide range of experimental conditions. They attributed this trend to the effect of out-of-plane puckering (Fig. 2C), as a result of low adhesion of the 2D materials to the substrate and increasingly high flexibility (low bending stiffness) of the 2D materials as the thickness decreases. Similar effects were observed in FFM experiments on CVD-grown graphene on copper [62] and chemically modified graphite [61]. Evidently, adhesion plays an important role in the nanoscale single asperity friction on the layered 2D materials, where the high flexibility of 2D layers makes it possible to deform significantly under the AFM tip, subject to both adhesive and frictional forces with the tip and the substrate. If the tip adhesion is relatively high, the top 2D layer could become delaminated as the tip is retracted, leading to an abnormal “negative” friction coefficient as observed on chemically modified graphite [61].

In addition to the noted effects of electron–phonon coupling and puckering, MD simulations have shown that the surface roughness of the substrate could also lead to thickness-dependent friction [73]. By simulating a capped carbon nanotube sliding on suspended graphene, Smolyanitsky et al. [74] suggested that the total lateral force resulted from two main contributors: one due to the pinning forces between the tip and graphene, and the other due to the deformation field within and outside the contact zone. It was found that the lateral energy corrugation resulted from the elastic strain energy associated with the deformation field in addition to the interactions between the tip and the

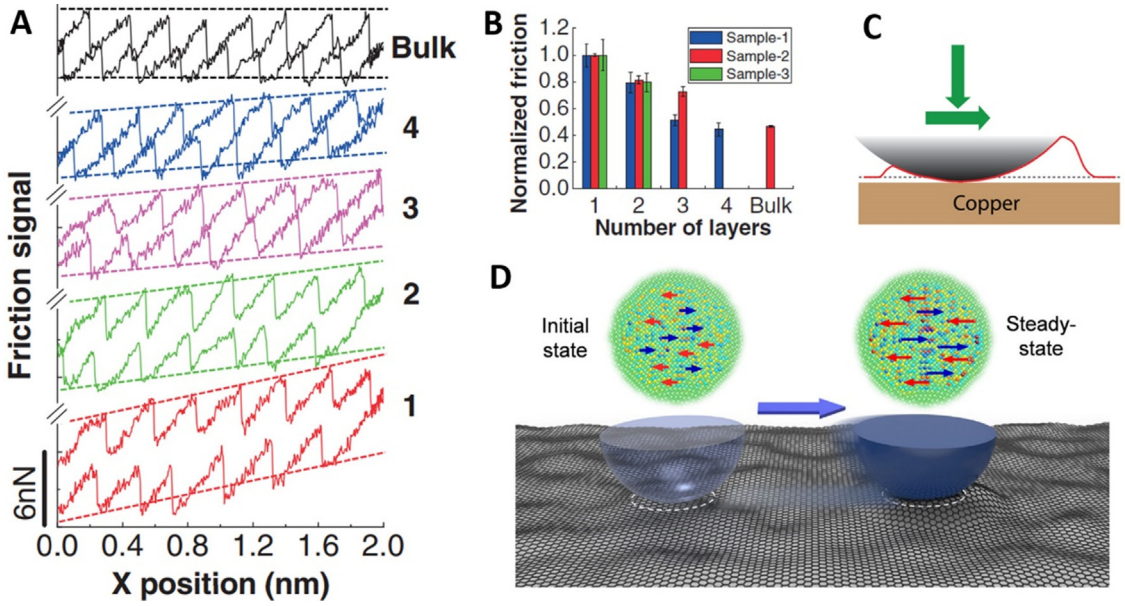

Fig. 2. (**A**) FFM measurements of thickness-dependent friction on graphene, showing friction force as a function of scan distance, with stick–slip motion and an unusual "strengthening" effect. The numbers on the right indicate the corresponding numbers of graphene layers. (**B**) Normalized friction on graphene with different layer thicknesses. (**A** and **B**) are adapted with permission from [60]. (**C**) Schematics of deformation of a 2D material subject to adhesion and friction forces under an AFM tip. Figure is adapted with permission from [62]. (**D**) A schematic showing the evolution of interfacial pinning forces. Figure is adapted with permission from [72].

top layer graphene [75,76]. Li et al. [72] conducted MD simulations to study the friction of a Si tip sliding on graphene supported by an amorphous Si substrate. Their simulations reproduced the observed strengthening effect and the thickness dependence, which they attributed to two key factors: the local pinning forces acting on the interfacial atoms and the overall commensurability of the interface. It was noted that the highly flexible 2D materials can dynamically adjust their configurations to change the strength and coordination of the local pinning forces as the tip slides (Fig. 2D). It remains unclear how these competing ideas may be correlated or corroborated.

Friction on chemically modified graphene was found to be higher than that on pristine graphene [77–81], where the change in the mechanical properties of graphene through chemical modification is likely less influential than the change in the local chemistry at the interface. For example, the near-surface energy corrugation increased significantly on a fluorinated graphene, largely due to the change in the bonding state of carbon from sp^2 to sp^3 [82] and the introduction of the highly polarized fluorine atoms [79]. As a result, both the static coefficient of friction and the average kinetic friction force increased substantially. It was also suggested that an increase in atomic-scale roughness on the surface of chemically modified graphene could increase friction [83]. However, surface roughening through chemical modification was observed to saturate at low coverages, and thus cannot fully explain the observed increase in friction. For graphene oxide [80,81], the higher friction was attributed to a greater number of intercalated functional groups leading to an increase in the interfacial shear strength. Thus, the interfacial chemistry and the associated mechanochemical interactions between the sliding surfaces should have a strong influence on the friction properties of chemically modified graphene and other 2D materials. Moreover, the mechanochemical interactions between the scanning probe and the 2D layers could also have a significant impact on the atomic scale wear during repeated sliding [84–86].

The effect of humidity was found to be insignificant in the FFM measurements on monolayer graphene [60,87], possibly due to the inert and relatively hydrophobic surface of graphene. However, it was found that humidity could lead to load-dependent friction hysteresis, with larger friction measured during unloading compared to loading for a given normal load [88]. MD simulations suggested that the friction hysteresis resulted from the water contact angle hysteresis at the tip-graphene interface. More recently, Gong et al. [89] showed that graphene exhibited higher overall friction and hysteresis in higher humidity conditions, with no hysteresis observed under dry conditions. In general, exposure to the ambient environment could lead to oxidation of the surface and change of surface energy, influencing both adhesion and friction.

FFM measurements of friction on 2D materials can be strongly affected by the supporting substrates [63,90,91]. When placed on top of crystalline substrates with similar lattice structures, 2D materials often form moiré superstructures with periodic surface undulation and local straining [92]. FFM signals on such surfaces often exhibit notable long-wave modulation coinciding with the periodic superstructures [93,94], which may be attributed to the height undulations [95]. As noted earlier, both the adhesion strength and the substrate surface roughness can affect the friction behavior of 2D materials. Zeng et al. [96] found that increasing adhesion of graphene to the substrate by plasma treatments of the substrate surface led to reduced friction, likely due to the suppressed puckering effect. Spear et al. [97] studied the effects of surface roughness and chemistry on the friction properties of monolayer and few-layer graphene using silica nanoparticle films with controlled nanoscale roughness and chemically modified surfaces. Their results emphasized the effects of graphene-substrate interactions and the tip size on the friction measurements of rough surfaces [91].

As a powerful tool for characterizing nanoscale friction of 2D materials, FFM measurements depend not only on the intrinsic interactions at the 2D-3D interfaces but also on the mechanical properties of the 2D materials as well as the supporting substrates and the probe tip. Moreover, the environmental effects such as humidity and temperature could be important as well as the surface roughness of the substrate, tip size/shape, and scan velocity. It is unclear what fundamental properties of the 2D-3D interfaces may be extracted directly from the FFM experiments. The static and kinetic friction coefficients in classical theory are apparently not applicable at the nanoscale, as the friction force often depends on the normal load nonlinearly. The atomic stick–slip behavior as measured by FFM could be related to the lateral energy corrugation near the surface of 2D materials. Meanwhile, the lateral

energy corrugation varies with the normal load, which may be related to the normal traction-separation relations for adhesive interactions at the interface. Thus, a 3D energy landscape near the surface may be used to describe both adhesion and friction interactions, although such an energy landscape could evolve dynamically in response to tip sliding and deformation of the 2D materials as well as the substrate and environmental effects. Furthermore, to scale up from the nanoscale single-asperity friction, it may be possible to define an interfacial shear strength as a key parameter for the shear interactions across a 2D-3D interface at larger scales. For example, a continuum mechanics analysis based on the Maugis–Dugdale or "transition" model was used to fit the measured friction forces versus normal loads on SiO_2 and graphene, from which the work of adhesion and interfacial shear strength were deduced [98]. Similarly, the Derjaguin–Mueller–Toporov (DMT) model was used to compare the shear strength and the work of adhesion of graphene on different substrates such as SiO_2 and Ni(1 1 1) [87]. Given environmental conditions, the interfacial shear strength would likely depend on the normal load (traction) and sliding rate. The substrate surface roughness may have a profound effect on the shear interactions, potentially size-dependent due to the statistics of the surface topology from atomistic to nano- and microscales. Further studies may help bridging the nanoscale friction by FFM measurements to shear interactions at micro- and macro-scales.

Besides FFM, shear interactions between 2D materials and their 3D substrates have been examined by deforming either the substrates or the 2D materials to induce relative sliding. Measuring the deformation of the substrate-supported 2D materials could then be used to infer the shear tractions at the 2D-3D interfaces. For example, monolayer graphene on a stretchable substrate can be strained by stretching the substrate (Fig. 3A), which transfers an axial stress into the graphene through interfacial shear tractions. By measuring the strain distributions in the graphene, e.g., by Raman spectroscopy (Fig. 3B), the interfacial shear traction between graphene and the substrate can be deduced from a shear-lag analysis [64–67]. In particular, Jiang et al. [65] assumed a linear relation between the interfacial shear traction and the relative sliding displacement followed by a constant traction as the interfacial shear strength in their analysis of microscale monolayer graphene flakes on a stretchable PET substrate. They obtained values of the graphene-PET interfacial shear strength between 0.46 and 0.69 MPa, much lower than those (~24 MPa) deduced from FFM measurements for the graphene-SiO_2 interface at the nanoscale [98]. Similar experiments by Xu et al. [66] found that the interfacial shear strength between graphene and the PET substrate is size-dependent, decreasing by two orders of magnitude when the graphene sample length was increased from ~20 μm to 10 mm. While the underlying mechanism remains unclear, the effect of multiscale surface roughness could be the key to understanding the size-dependent interfacial shear strength. Other studies found that the graphene-polymer interfacial shear strength was tunable by the number of H-bonds [27,67]. Interestingly, the interfacial shear interactions were related to cracking of polycrystalline CVD graphene on copper foil under tension [68], where regularly spaced cracks in graphene were observed. The spacing between the cracks decreased with increasing strain applied to the copper foil until a minimum spacing was reached. The minimum crack spacing (~3 μm) was related to the graphene-copper interfacial shear strength by the shear lag analysis, yielding a value of ~0.49 MPa.

Kawai et al. [69] investigated the friction behavior of graphene nanoribbons (GNRs) on an Au(1 1 1) substrate (Fig. 3C) using dynamic AFM in UHV at a low temperature (4.8 K). By dragging the GNRs back and forth in a controlled manner, they reported static friction forces in the order of 100 pN for GNRs with lengths ranging from 3 to 22 nm (Fig. 3D), and the static friction force per unit length was found to decrease with increasing length. With an estimated width of ~2 nm for the GNRs, the interfacial shear strength between graphene and the Au (1 1 1) substrate can be estimated from the measured static friction forces at ~16 to ~0.5 MPa. At the nanoscale with the atomically smooth Au(1 1 1) surface, the size dependent friction may be attributed to the pinning effect at the nanostructured edges of the GNRs.

Deformation of 2D materials by pressure difference has been used to characterize mechanical and interfacial properties, including adhesion [21,22] and shear [70,71]. By pushing the suspended graphene into a circular micro-chamber under variable external pressures (Fig. 3E), Kitt et al. [70] showed that the supported graphene outside the chamber was stretched and slid over the substrate. Based on Raman spectroscopy and a continuum membrane model, they extracted the pressure-dependent sliding friction (interfacial shear strength) between the silicon

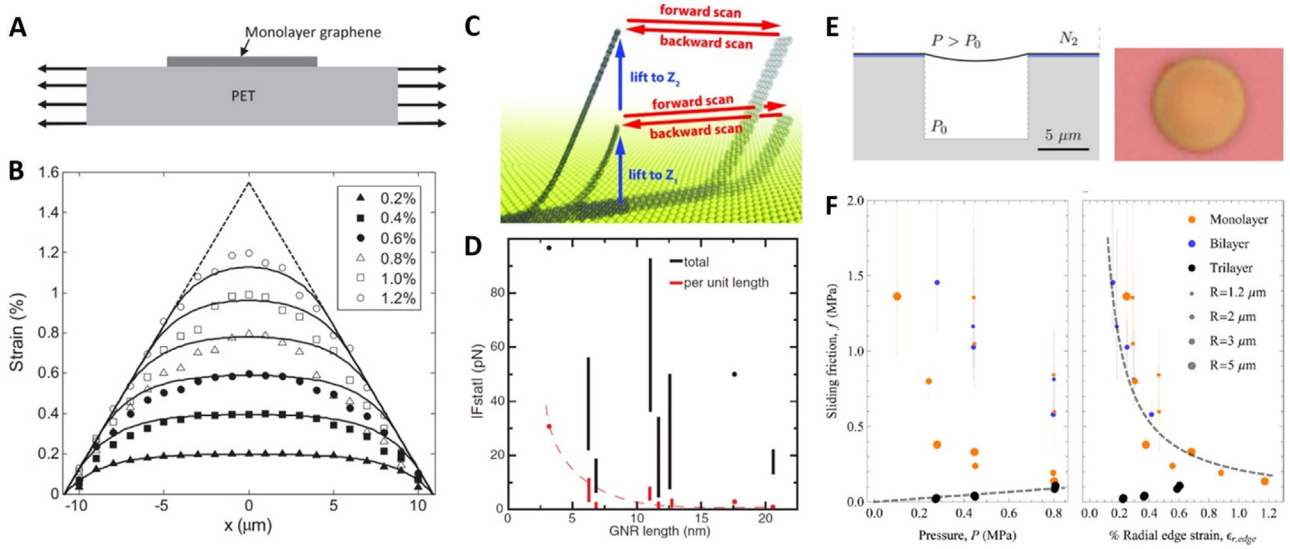

Fig. 3. (**A and B**) Schematic of a graphene monolayer on a PET substrate being stretched, with strain distributions in graphene measured by Raman spectroscopy (symbols) and predicted by a nonlinear shear lag analysis (lines). Figures are adapted with permission from [65]. (**C and D**) Schematic of lateral manipulation of graphene nanoribbons on an Au(1 1 1) substrate, with the measured static friction force (F_{stat}) (black) and F_{stat} per unit length (red) versus the GNR length. Figures are adapted with permission from [69]. (**E and F**) Cross-section schematic showing a microchamber etched into the underlying Si substrate and the supported graphene atop, and an optical image of a trilayer graphene-sealed microchamber; Sliding friction (shear strength) extracted as a function of applied pressure (left) and as a function of the radial strain at the edge of the microchamber (right). The size of each data point represents the radius of the microchamber. Figures are adapted with permission from [70].

oxide substrate and mono-, bi-, and trilayer graphene (Fig. 3F). The interfacial shear strength for trilayer graphene was found to be proportional to the applied pressure, yielding a positive coefficient of friction (~0.12). In contrast, the friction shear strength for monolayer and bilayer graphene did not follow a linear relation and instead was found to be inversely proportional to the radial strain in the graphene. The strain dependence was attributed to the high surface conformation enabled by the low bending rigidity and strong adhesion of graphene to the substrate. The shear strength for monolayer graphene ranged from 0.1 to 1.5 MPa, with no clear dependence on the chamber radius (1.2–5 μm). More recently, Wang et al. [71] reported measurements of both the interfacial and interlayer shear strengths of graphene based on pressurized micro-bubbles. By controlling the internal pressure, they observed continuous growth of an interfacial shear zone outside the bubble edge and extracted an interfacial shear strength of ~1.64 MPa between monolayer graphene and the silicon oxide substrate, whereas a much lower interlayer shear strength of ~0.04 MPa was obtained from bilayer graphene bubbles.

2.3. Mixed-mode interactions

Mechanics at the 2D-3D interfaces is generally complicated with coupled normal (adhesion) and tangential (friction/shear) interactions. Such coupling effects have been noticed in interfacial fracture experiments to measure the adhesion energy or interfacial toughness of 2D materials [35,36,99] as well as in the FFM experiments to measure nanoscale friction of 2D materials [60–62,87,91]. An intimate relationship between adhesion and friction may be established for the 2D-3D interfaces by considering the effects of mixed-mode interactions during adhesion/separation and sliding processes.

Following the mixed-mode fracture mechanics of bi-material interfaces [100], the phase angle (ψ) of the mode-mix can be defined by the ratio of the shear traction (τ) to the normal traction (σ) at an interface, i.e., $\tan\psi = \tau/\sigma$. The mode-mix ranges from pure mode I (opening mode, $\psi = 0$) to pure mode II (shearing mode, $\psi = \pm 90^{\circ}$) in fracture experiments where the normal traction is tensile ($\sigma > 0$). For sliding friction, typically with a compressive normal traction ($\sigma < 0$), the phase angle of interaction mode-mix ranges from 90° to 270°, with a phase angle of 180° for pure contact mode with no shear ($\tau = 0$). For example, the pressurized blister tests are inherently mixed mode with both normal and shear tractions at the interface. As a result, it is possible to determine both the adhesion energy [21,22] and the interfacial shear strength [70,71] of 2D materials by the blister tests. By varying the mode-mix in their blister tests with a backing layer, Cao et al. [35] showed that the interfacial toughness between graphene and substrates (Cu and Si/SiO_2) increased with increasing shear components, similar to interfacial fracture between bulk materials, likely due to the effect of asperity locking with the substrate surface roughness [101]. On the other hand, the pressure-dependent interfacial shear strength between graphene and the SiO_2 substrate [70] is an evidence of mixed-mode interactions in the regime of negative normal tractions ($90^{\circ} < \psi < 270^{\circ}$).

The traction-separation relations (TSRs) used to describe the adhesive interactions ($\psi = 0$) may be extended to mixed-mode interactions. For example, Cao et al. [36] extracted the mixed-mode TSRs from pressurized blister tests, where CVD-grown monolayer graphene backed by a photoresist film was transferred to a highly polished copper substrate. A range of mode-mix phase angles ($-84^{\circ} < \psi < -27^{\circ}$) were achieved by varying the photoresist thickness. Combining measurements of the blister deformation profiles and normal crack opening displacements with a cohesive zone model, mixed-mode TSRs were deduced for the graphene-copper interface. While these results demonstrated the mixed-mode interactions during fracture of the graphene-copper interface, further studies are needed to unveil the coupling mechanisms and to unify the normal (adhesive) and shear (frictional) interactions within a general framework of mixed-mode interactions at the 2D-3D interfaces.

3. 2D-2D interfaces

As a common feature among various 2D materials, the relatively weak vdW interactions are the primary forces acting between adjacent layers in contrast to the strong intralayer bonding, rendering a family of highly anisotropic vdW layered materials [102]. The interlayer binding energy as calculated from various DFT methods ranges from 20 to 120 meV/atom for a variety of 2D materials, about two orders of magnitude weaker than the intralayer binding energy. The equilibrium interlayer separation is typically 3–7 Å. However, direct measurements of the 2D-2D interactions are challenging, especially for the interactions between different types of 2D materials in vdW heterostructures [1–3]. In this section, we discuss recent advances in the study of the mechanical interactions between 2D materials and related interlayer phenomena of vdW structures.

3.1. Interlayer adhesion and normal interactions

3.1.1. Interlayer adhesion

The interlayer adhesion energy due to vdW interactions is typically expected to be on the order of 100 mJ/m^2, consistent with an interlayer binding energy of 20–120 meV/atom. As listed in Table 2, measurements of the interlayer adhesion energy are relatively scarce. Liu et al. [103] presented an experimental method to measure the graphene-graphene interlayer binding energy (190 ± 10 mJ/m^2) with a sequence of delicate mechanical manipulations by sliding, twisting and bending of highly oriented pyrolytic graphite (HOPG) flakes. The interlayer adhesion leads to a self-retraction phenomenon, based on which Wang et al. [104] measured an interlayer adhesion or cleavage energy of graphite, with a value of 370 ± 10 mJ/m^2 for the incommensurate state of bi-crystal graphite and a slightly higher value of 390 ± 20 mJ/m^2 for the ideal ABAB stacking. Similarly, by measuring the shear force at the onset of sliding of HOPG mesa structures, Koren et al. [105] reported an interlayer adhesion energy of 227 ± 5 mJ/m^2. Such measurements typically assume negligible friction between the layers, which may be justified for incommensurate stacking with superlubricity as discussed further in Section 3.2. Alternatively, the presence of spontaneously formed nanoblisters in layered 2D materials offers an indirect method for a quick estimate of the interlayer adhesion energy by measuring the aspect ratios of the nanoblisters [30,106]. A particular convenience of this method is that nanoblisters commonly form when transferring and stacking 2D layers due to contamination in the form of gas molecules or liquid trapped between the layers [107,108]. Based on measurements of the nanoblisters in various 2D materials including vdW heterostructures, both interfacial (2D-3D) and interlayer (2D-2D) adhesion energies were determined (Fig. 4A) [30], ranging from 50 to 250 mJ/m^2. Remarkably, even atomic-scale blisters

Table 2
Measurements of 2D-2D interlayer adhesion/separation energies of various 2D materials (G for graphene; A and S denote adhesion and separation, respectively).

2D Materials	Adhesion Energy (mJ/m^2)	Method	Ref
G–hBN hBN–hBN MoS_2–hBN G–MoS_2 MoS_2–MoS_2	126 ± 20 (A) 129 ± 4 (A) 136 ± 11 (A) 140 ± 26 (A) 174 ± 18 (A)	Spontaneous nanoblisters	[30]
G–G	86 ± 16 (A)	Spontaneous nanoblisters	[30]
	221 ± 11 (S)	Atomic intercalation	[109]
G-G	190 ± 10 (A)	Deformation over a step	[103]
Graphite-Graphite	227 ± 5 (S) 370 ± 10 (S)	Shearing	[105] [104]

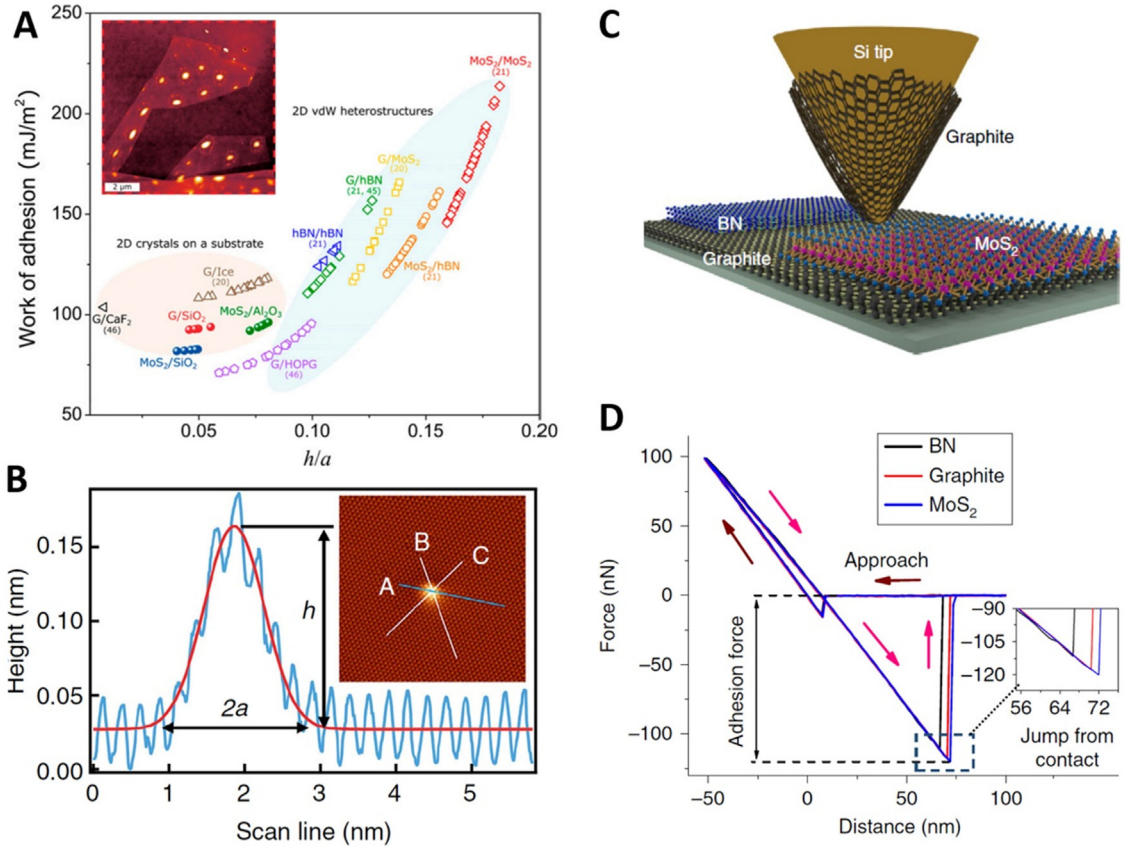

Fig. 4. (**A**) Adhesion energy of various 2D-2D and 2D-3D interfaces determined by measured aspect ratios (height/radius) of nanoblisters. The inset shows a tapping-mode AFM image of nanoblisters trapped between monolayer graphene and SiO_2. Figure is adapted with permission from [30]. (**B**) The height profile along the scan line A in the STM image (inset) of an atomic-scale blister formed by intercalating neon atoms into the graphene-graphite interface. Figure is adapted with permission from [109]. (**C**) Schematic illustration of an AFM tip wrapped with a thin graphite layer in contact with BN, MoS_2 or graphite. (**D**) Typical approaching and retracting force–displacement curves measured by a graphite-coated AFM tip on BN, MoS_2, and graphite. The inset enlarges the view to highlight the critical detaching forces. (**C** and **D**) are adapted with permission from [112]

as created by neon atom intercalations could be used to measure adhesion energy of graphene atop HOPG (Fig. 4B) [109]. These measurements have benefited from a simple analytical model considering the mechanics of 2D materials including bending and stretching deformations [110,111].

Recently, Li et al. [112] probed the vdW interactions between three pairs of 2D materials (graphene-graphene, graphene-hBN, and graphene-MoS_2) using a graphite-wrapped AFM tip (Fig. 4C). They found that, compared to graphene-graphene adhesion, graphene-hBN adhesion is weaker and graphene-MoS_2 adhesion is stronger. The critical adhesion forces were measured from force-distance curves (Fig. 4D), typically with a jump-in during approach and a pull-off during retraction. However, because it was not possible to precisely determine the contact area between the graphite-wrapped AFM tip and the substrate, the adhesion energy between the 2D materials could not be determined quantitatively. Nevertheless, the relative strengths of the adhesive interactions among the three pairs were found to be consistent with the prediction based on Lifshitz theory [112], considering the effect of material dielectric functions on the 2D-2D vdW interactions. Based on the relative adhesion strengths, it was demonstrated that MoS_2 could be used as a manipulator to pick up graphite or graphene from hBN substrates [112].

The key to realizing the potential of vdW structures lies in the ability to achieve the deterministic stacking of 2D layers in specific sequences and orientations [1–3]. The fabrication would have to involve extensive transfer processes [113], including exfoliation of 2D materials from their bulk crystals and transfer from donor to target substrates, where the adhesive interactions are at play. In particular, it is believed that hBN can develop robust adhesion with other 2D materials [14]. A so-called vdW pick-up transfer method has been widely adopted by using an hBN flake (instead of elastomer) as the stamp to pick up a 2D material from its substrate and then transfer the hBN-caped 2D material [107,113]. In contrast to polymer-based wet or dry transfer methods, this method could lead to hBN-encapsulated vdW structures with clean interfaces as the 2D materials were not directly exposed to polymers throughout the transfer process [113,114]. Even hydrocarbon and water contamination absorbed on 2D material surfaces during the exfoliation procedure could be suppressed by the 2D-2D interactions into nano-blisters [30,115], which can be further squeezed out via thermal or mechanical treatments [107,116,117]. In addition, hBN flakes could act as an atomically flat insulator and thus address a critical issue that the electronic performance of 2D materials degrades significantly when supported by amorphous SiO_2 [14]. This technique was initially developed for hBN-encapsulated graphene devices and has proved to be useful for building other vdW structures with a number of different 2D materials in the stack [14].

3.1.2. *Interlayer compression*

In addition to adhesion and separation, where the interlayer vdW forces are predominantly attractions, repulsive interactions between the 2D layers can be activated by compression. Several recent studies reported a tight coupling between the interlayer deformation and the physics and chemistry of the vdW structures [118–121]. For example, Yankowitz et al. [13] employed a piston-cylinder pressure cell to controllably tune the interlayer separation in graphene-hBN heterostructures (Fig. 5A). By increasing pressure to decrease the interlayer

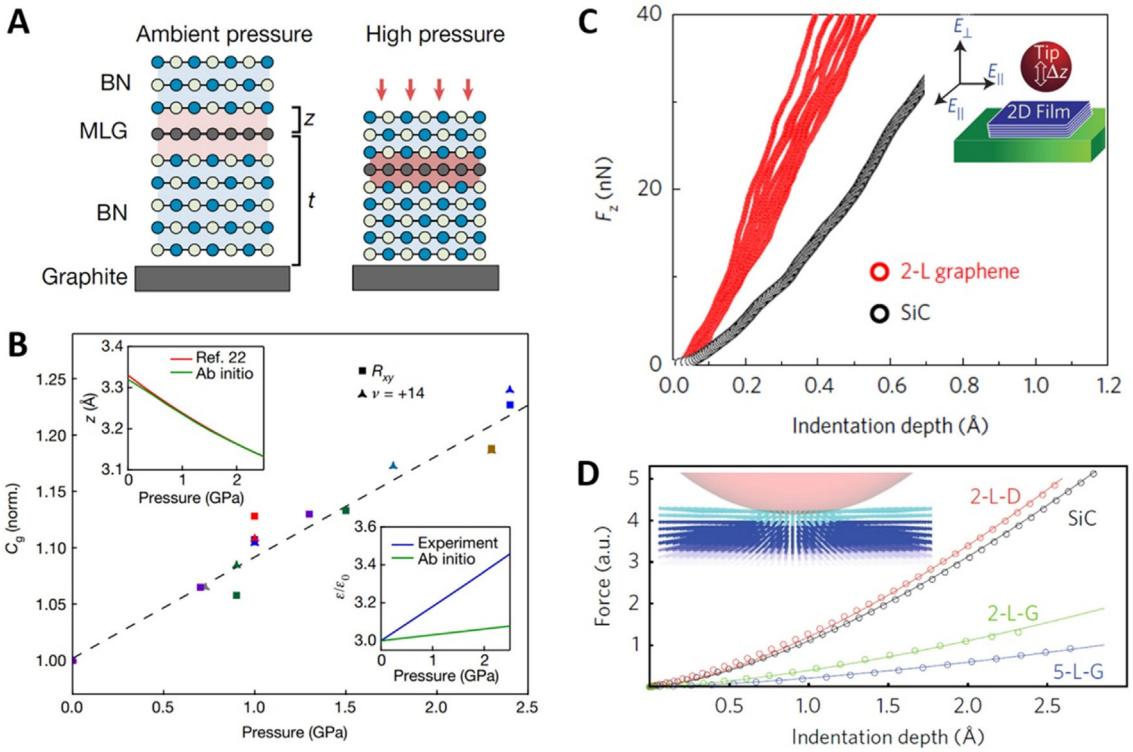

Fig. 5. (**A**) Schematic of a vdW heterostructure made of a monolayer graphene encapsulated between two hBN flakes under ambient and high pressure. (**B**) The gate capacitance as a function of pressure, normalized to its value at 0 GPa for each device. Top inset: change in hBN interlayer spacing as a function of pressure predicted by ab initio calculations (green curve), in comparison with measurements by X-ray diffraction (red curve). Bottom inset: increase of the hBN dielectric constant from experiments (blue curve) and ab initio calculations (green curve). (**A** and **B**) are adapted with permission from [13]. (**C**) Indentation curves on 2-L epitaxial graphene (red) and SiC (black), showing an ultrastiff phase in 2-L graphene at room temperature. Inset: schematic of the sub-ångström indentation on 2D materials. (**D**) Indentation curves calculated by DFT, for a bare substrate (SiC) and for the same substrate coated with a 2-L diamond-like film (2-L-D) or graphene (2-L-G), as well as a 5-L graphene (5-L-G). Circles show calculated data, and solid lines show fitting with a Hertz contact model. Inset: a spherical indenter (pale red) pressing on a substrate (blue) coated with a thin film of a stiffer material (cyan). (**C** and **D**) are adapted with permission from [118]. Inset in (**C**) is adapted with permission from [122].

separation, they observed a significant increase in the gate capacitance (Fig. 5B) along with a superlinear increase in the bandgaps, indicating pressure-enhanced electronic coupling between the 2D layers [13]. More recently, Yankowitz et al. [8] showed that hydrostatic pressure could be used to tune the phase diagram of twisted bilayer graphene and to shift the superconducting transition to higher twist angles and higher temperatures. Moreover, it has been reported that the magnetic order in atomically thin 2D magnets, e.g., CrI_3, could be drastically modified by pressure [120,121]. With a hydrostatic pressure up to 2 GPa, Li et al. [120] observed an irreversible interlayer antiferromagnetic-to-ferromagnetic transition in CrI_3, accompanied by a monoclinic-to-rhombohedral stacking-order change. Before the structural change, the interlayer antiferromagnetic coupling could be tuned up drastically by the hydrostatic pressure.

These appealing effects of interlayer coupling with physical properties of vdW materials make it necessary to understand repulsive interlayer forces when the 2D layers are compressed into closer proximity (e.g., $\delta_n < \delta_0$ in Fig. 1A). In this regime, the 2D-2D interactions could be strongly influenced by the atomic structures of 2D materials and their stacking orders. Atomic-scale deformation and structural transformation could be induced mechanically (e.g., by hydrostatic pressure or indentation), leading to tunable electronic and magnetic properties. To probe the mechanics of interlayer elasticity in vdW structures, Gao et al. [122] conducted sub-ångström-resolution indentation measurements of supported 2D materials including few-layered graphene and graphene oxide films. They found that the interlayer elasticity was highly sensitive to the presence of intercalated molecules in between the layers. In particular, the interlayer elastic modulus of the graphene oxide films depended on the relative humidity and reached a maximum with one complete layer of water molecules intercalated between the graphitic layers [122]. By the same indentation method, Gao et al. [118] showed that epitaxial bilayer graphene on SiC(0 0 0 1) exhibited a diamond-like transverse stiffness and hardness (Fig. 5C), along with a reversible drop in electrical conductivity. Their DFT calculations suggested an indentation-caused sp^2-to-sp^3 chemical transition in bilayer graphene, producing a diamond-like film with increased stiffness (Fig. 5D). Similarly, Yankowitz et al. [123] applied a local pressure with an STM tip to aligned or nearly-aligned graphene on boron nitride and found that modifying the interlayer separation could induce locally commensurate stacking underneath the tip. Further studies should consider the interplay between pressure, interlayer registry, and the in-plane and out-of-plane deformations of the 2D layers, with spatially non-uniform, multiscale features (such as strain solitons). A better understanding of the interlayer forces would be particularly beneficial to achieve tunable properties and functionalities of the vdW structures.

3.2. Interlayer friction and shear interactions

The fabrication and applications of vdW structures often depend on and sometimes can benefit from the unique friction and shear properties of 2D-2D interfaces. Examples include the alignment of graphene on hBN via self-rotation and the emerging devices based on twisted 2D materials. An understanding of the interlayer shear interactions would be of importance, in particular between monolayer 2D materials – such as twisted bilayer homo- or heterostructures that have been the source of recent excitements enabling a host of novel photonic and electronic devices [4–11,124].

3.2.1. Interlayer friction and superlubricity

It has been well known that the interlayer friction is low in vdW materials, a common feature due to weak vdW interactions between atomically smooth crystal planes. For this reason, many of their bulk counterparts, such as graphite, hBN (also called white graphite), MoS_2 and WS_2, have been used practically as solid/dry lubricants. However, detailed characterization and understanding on the interlayer friction and shear interactions between various 2D vdW materials have not been achieved until recently, with the development of AFM-based metrologies and the fabrication of large pristine single-crystal 2D materials [59,63,125]. Miura et al. [126] first reported measurement of sliding friction between MoS_2 flakes and bulk MoS_2 substrates. They found that the friction forces were proportional to the normal loading forces, following classic Amontons-Coulomb law with an ultralow friction coefficient of about 0.003. Adopting a similar approach, they reported anisotropic friction of graphite flakes on graphite [127], with a friction coefficient of approximately 0.001 for sliding along the $[1\ 2\ \bar{3}\ 0]$ direction of the graphite basal plane. Using a home-built friction force microscope, Dienwiebel et al. [128] measured atomic-scale friction as a function of the rotational angle between two graphite layers. They reported a periodic friction behavior (Fig. 6A): the friction force was extremely small (below experimental error) except for narrow ranges near the commensurate stacking states with an angular periodicity of ~60° [128]. They attributed the ultralow friction to the incommensurability between the rotated graphite layers, an effect of "superlubricity" as proposed originally by Hirano and Shinjo [129]. The atomistic origin of the ultralow interlayer friction could be conceptually understood by an egg-box foam model [125] or a glued ping-pong ball model [130]. When two atomic planes slide against each other, some of the atoms climb uphill and some go downhill such that the overall friction force cancels out (as long as the planes are sufficiently large and their contact is not too close to the commensurate registry). The term, structural superlubricity, has also been used to describe the vanishingly small friction with incommensurate crystalline contacts. Apparently, such structural superlubricity has become a common feature of the atomically smooth 2D-2D interfaces, as evidenced by recent experiments based on graphite [105,131] and MoS_2 [132,133] as well as a number of vdW heterostructures, including graphene/hBN [6,134], WS_2 on graphene and hBN [135,136], graphene/MoS_2, graphene/TaS_2 and graphene/ReS_2 [137]. Notably, the robustness of structural superlubricity can benefit from interfacial heterogeneities in the heterostructures due to the presence of lattice mismatch and hence intrinsic incommensurability.

To examine the friction of heterostructured interfaces under high normal load in ambient conditions, Liu et al. [138] employed multilayer graphene-coated SiO_2 microsphere (GMS) probes to slide on bulk HPOG and hBN under high contact pressures (Fig. 6B). They reported a friction coefficient of 0.003 on HPOG and 0.0025 on hBN, where the ultralow friction was attributed to the overall incommensurability with multi-asperity contact and randomly oriented graphene grains. The experimental results suggested that superlubricity could be achieved at the microscale with multi-asperity contacts of heterostructured interfaces. This method was recently extended to measure the friction of other 2D heterostructured interfaces with single-crystalline contact, using various 2D flake-wrapped AFM tips (i.e. graphite-, hBN-, MoS_2-, ReS_2-, and TaS_2-wrapped tips) [137]. A friction coefficient as low as 0.0001 was reported for the hBN/graphite interface. Remarkably, the measured lateral force map between ReS_2 flakes displayed hexagonal patterns with atomic resolution [137].

The electronic properties of 2D heterostructures depend on the

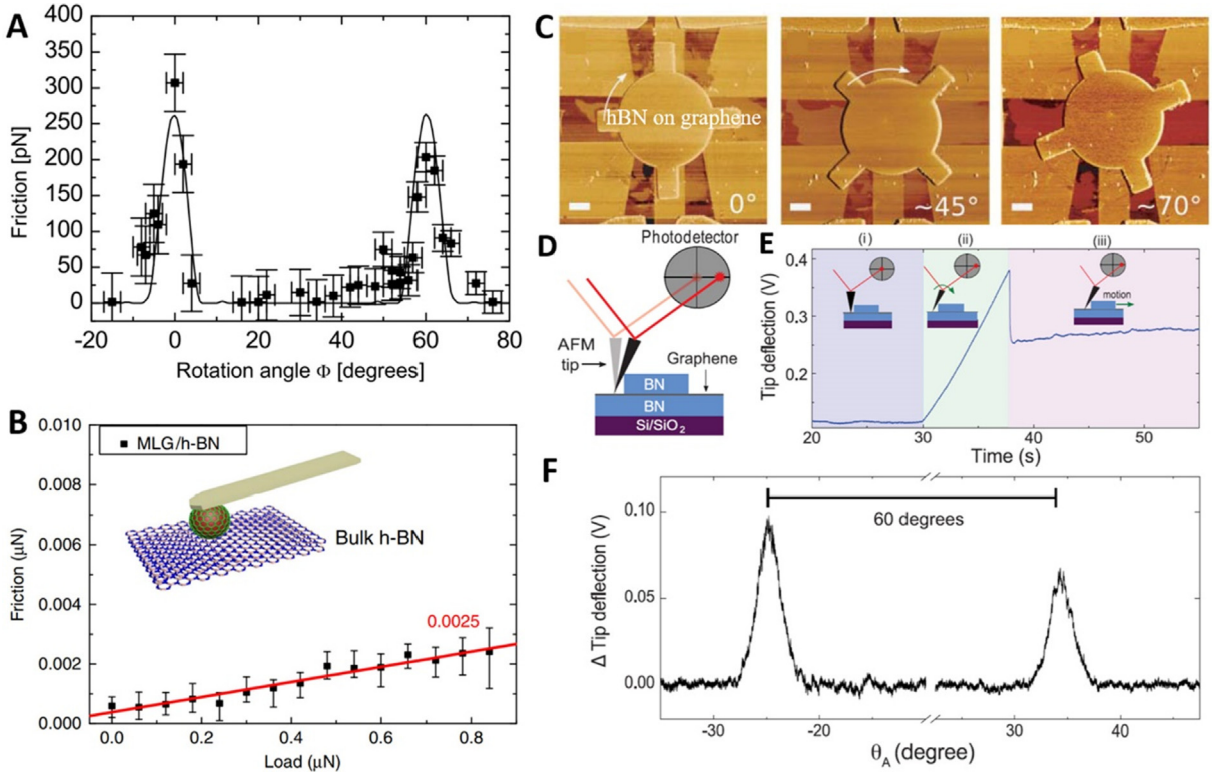

Fig. 6. 2D-2D interlayer friction and shear interactions. (**A**) Average friction force versus rotation angle of the graphite samples, with ultralow friction for a wide angular range between two narrow peaks at 0 and 61°. The solid curve shows results from a model calculation. Figure is adapted with permission from [128]. (**B**) Friction force as a function of normal load for graphene/hBN measured by using a graphene-coated microsphere. The inset is a schematic of the friction test. Figure is adapted with permission from [138]. (**C**) AFM images of a micro-patterned hBN wheel on graphene with three different orientations. Scale bars: 1 μm. (**D**) Schematic of friction measurement using an AFM tip. (**E**) Tip deflection versus time in a translational push of the upper hBN, with three different regimes of friction: (i) tip-substrate friction, (ii) static friction, and (iii) dynamic friction. (**F**) Tip deflection (an indicator of friction force) versus absolute angle, measured during continuous rotation of the hBN wheel. (**C–F**) are adapted with permission from [6].

interlayer coupling and can vary dramatically with relative rotation. This effect was recently demonstrated by a device architecture with rotatable hBN/graphene heterostructures (Fig. 6C), where friction of the top hBN on graphene was measured (Fig. 6D–F) [6]. With a translational push, both static and steady-state dynamic friction were observed (Fig. 6E). With continuous rotation, two peak friction forces were observed with a separation of 60° (Fig. 6F), resembling the transition from superlubricity (incommensurate stacking) to a commensurate state in graphite [128]. However, because of the lattice mismatch between graphene and hBN, there should not be any true commensurate lattices at any angle, and thus the increased friction should result from a different origin, for which the moiré superlattice formed in the rotated heterostructure was alluded to as a possible cause. In separate studies, Song et al. [134] found that the friction anisotropy in the graphite/hBN heterojunction was much smaller than that for homogeneous graphitic contacts. Their atomistic simulations revealed that the friction anisotropy in the heterojunction originated mainly from the internal lattice deformation of the 2D layers. More specifically, in the aligned configuration, the heterostructure exhibited significant out-of-plane undulations with soliton-like patterns. Such undulations rapidly decay upon rotation to a misaligned configuration. In contrast, the rotation angle dependence of friction between graphite and hBN was not observed in the experiments using graphene-coated microspheres [138] or graphite-wrapped AFM tips [137].

3.2.2. Interlayer shear

In addition to friction forces and friction coefficients, measurements of the interlayer shear strength between different 2D materials have been reported. Based on Raman spectroscopy and pressurized blister devices, Wang et al. [71] obtained an average value of ~0.04 MPa for the graphene-graphene interlayer shear strength, which is in the same order as the inter-tube friction in multi-walled carbon nanotubes [139]. By in situ mechanical shearing tests on cross-section TEM samples of MoS_2 flakes, Oviedo et al. [133] obtained an interlayer shear strength of 25.3 ± 0.6 MPa in the [120] direction at zero normal pressure. While this value compares closely with the shear strength of sputter deposited MoS_2 films at zero contact pressure [140], much smaller values (~0.02–0.12 MPa) were obtained for the interlayer shear strength from the friction tests between incommensurate MoS_2 monolayers (contact area ~0.3–7.9 μm^2) using a Si nanowire force sensor [132]. Similarly small values of shear stress were reported for microscale monocrystalline graphite/hBN heterojunctions (contact area ~9 μm^2) [134]. Notably, the frictional shear stress for the graphite/hBN heterojunction was found to be nearly independent of the normal load (up to 100 μN or ~11 MPa), but increased slowly with the sliding velocity in agreement with the theory of thermally activated friction [141].

A simple relation between the shear strength and the friction force may be written as: $F = \tau_0 A - \mu \int \sigma dA$, where F is the friction force, τ_0 is the shear strength at zero normal load, σ is the normal stress, μ is the friction coefficient, and A is the contact area. However, in some friction experiments including FFM, the contact area cannot be determined precisely. It is also challenging to measure the normal stress, which may not be uniformly distributed over the contact area, although the total normal load ($N = -\int \sigma dA$) can be measured. Theoretically, the normal stress can be related to the normal separation by a traction-separation relation due to interlayer adhesive interactions. The friction coefficient then couples the normal (adhesive) interactions with the shear interactions. Both the friction coefficient and the shear strength are anisotropic in general. As shown in Fig. 6B, the friction coefficient is often determined as the slope of the friction force versus the normal load [138]. However, the contact area in this case may depend on the normal load. Assuming a linear dependence, $A = A_0 + N/q$, where A_0 is the contact area at zero normal load, the friction force depends on the normal load linearly as: $F = \tau_0 A_0 + (\mu + \tau_0/q)N$. Thus, the slope of the $F - N$ curve is actually greater than the friction coefficient and depends on the shear strength as well as the contact modulus (q). With a detailed analysis of contact, adhesion and shear interactions, both the friction coefficient (μ) and the shear strength (τ_0) could be determined from the friction experiments.

3.2.3. Modeling and simulations

To understand observed superlubricity between two graphite layers [128], Verhoeven et al. [142] employed a modified 2D Tomlinson model to calculate friction forces between a finite, nanometer-sized, rigid graphene flake and a rigid monolayer graphene as the graphite surface, assuming pairwise Lennard-Jones (LJ) interactions between the two graphene layers. They found good agreement between the calculations and the experiments (Fig. 6A). Matsushita et al. [143] conducted MD simulations of friction between clean graphite surfaces, where the interlayer interactions were modeled by the LJ potential and the intralayer interactions by a linear spring potential. They reproduced atomic-scale stick–slip motion with relatively low friction coefficients, as the bilayer system was kept in commensurate stacking with negligibly small intralayer deformation. They argued that the low friction coefficients resulted from the cancellation of the forces between two types of lattice sites in graphene. More recently, it was found that the pairwise LJ potential underestimated the energy corrugation for the interlayer shear interactions in graphitic systems [144]. With a combination of long-ranged vdW and short-ranged orbital overlap contributions, Kolmogorov and Crespi [144] proposed a registry-dependent interlayer potential (called the KC potential), which has since been used widely in modeling friction and interactions between graphene layers [145–148]. Similar interlayer potentials (ILPs) have also been developed for other 2D systems, such as graphene/hBN [149] and hBN/hBN [150].

Early studies on interlayer friction often assumed rigid layers or flakes with no intralayer deformation as in the 2D Tomlinson model [142,147]. The in-plane deformation was considered in a 2D Frenkel-Kontorova-Tomlinson (FKT) model by Gyalog and Thomas [153], who investigated the mechanism of atomic friction between two atomically flat surfaces with quadratic symmetry (square lattices). They predicted interesting features such as the formation of domains and irreversible jumps of topological defects during the sliding process but did not consider any specific 2D materials. More recent studies have considered both in-plane and out-of-plane deformations in bilayer graphene and vdW heterostructures [145,146,151,152,154,155]. Using a multiscale computational scheme, Kumar et al. [154] predicted that significant in-plane strains and the out-of-plane deflections can be introduced by interlayer forces in three bilayer structures (graphene-hBN, MoS_2-WS_2 and $MoSe_2$-WSe_2). An analytical form of periodic interlayer potential was developed based on ab-initio DFT calculations and used in conjunction with a nonlinear elastic plate model to predict both the interlayer and intralayer deformations. Due to the hexagonal symmetry of the interlayer potential, the bilayer graphene could form commensurate domains with alternating AB/BA stacking separated by incommensurate domain walls (Fig. 7A), depending on the applied strain [151]. Zhang and Tadmor [146] proposed a discrete–continuum (DC) method for the interlayer potential in bilayer graphene that included full atomistic resolution (discrete) in the short range with the KC potential and a continuum integral approximation in the longer range. Their simulations of twisted bilayer graphene showed that structural relaxation led to localized intralayer deformations within each moiré supercell (Fig. 7B) [145]. Although these studies did not focus on friction or superlubricity, the interlayer shear interactions are essential for the formation of the peculiar microstructures in bilayer 2D materials and heterostructures.

Mandelli et al. [155] performed fully atomistic simulations of a finite graphene flake sliding on graphene and hBN substrates. They showed that the commensurate graphene/graphene interface exhibited stick–slip motion with size-independent friction coefficients. In contrast, the graphene/hBN interface transitioned from stick-slip motion to smooth sliding as the flake size increased, which was attributed to the

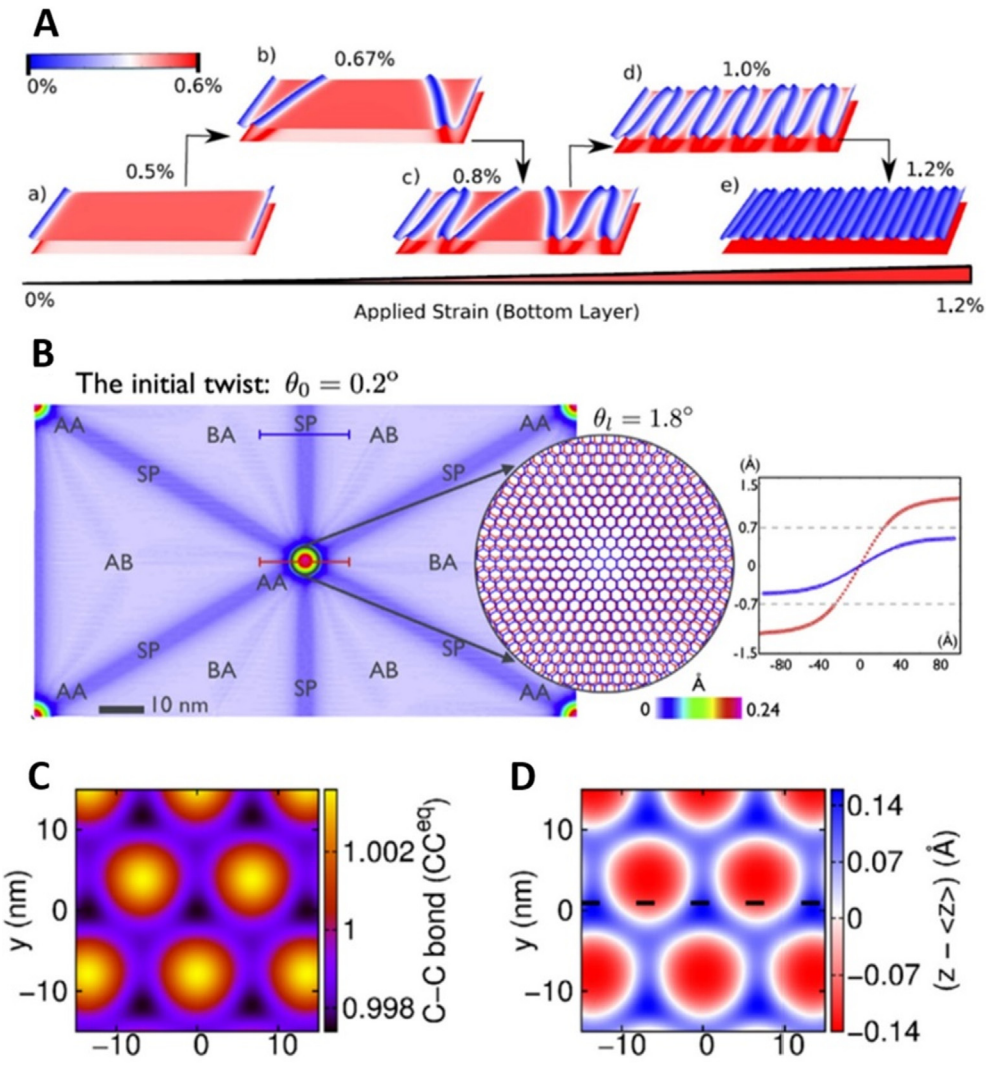

Fig. 7. Modeling of strain solitons and moiré superstructure in bilayer 2D materials. (**A**) In-plane strain patterns in a graphene bilayer as the bottom layer is subjected to different strains. Figure is adapted with permission from [151]. (**B**) A contour plot of the out-of-plane displacement in the top layer of a twisted graphene bilayer after relaxation. The inset shows a zoomed view of the atomic structure of the AA domain at the center of the cell. The graph on the right shows the relative shift between the atoms in the top and bottom layers along lines that cross the AA (red) and SP (blue) domains. Figure is adapted with permission from [145]. (**C–D**) Colored maps of the average carbon–carbon distance (in units of the equilibrium bond-length) and out-of-plane deflection after relaxation of a graphene layer over hBN at zero normal load. Figures are adapted with permission from [152]. (For interpretation of the references to colour in this figure legend, the reader is referred to the web version of this article.)

formation of moiré superstructure due to the lattice mismatch. Superlubricity set in as a result of smooth soliton-like gliding of the elevated ridges (domain walls) in the moiré superstructure (Fig. 7C and D). Moreover, negative friction coefficients were predicted for the graphene/hBN heterojunctions, resulting from the normal load-induced suppression of the out-of-plane distortions in the moiré superstructure [152]. Interestingly, it was found that thermally induced out-of-plane fluctuations led to an unusual increase of friction with temperature, in contrast with the theory of thermally activated friction [141].

The sliding dynamics of the edge-pulled graphene nanoribbons on rigid graphene and hBN monolayers was simulated recently by Ouyang et al. [156], using nonequilibrium MD simulations. They found that the interplay between the in-plane ribbon elasticity and the interfacial registry resulted in anisotropic snake-like motions. A nonlinear dependence of the friction force on the ribbon length was predicted, with a linear increase followed by saturation of the friction force above a characteristic length. Such sliding behavior is yet to be observed in experiments.

3.3. Interlayer phenomena

A particular feature of 2D-2D interfaces is their atomic level smoothness. This feature enables effective contact between 2D layers and unique interactions associated with relative interlayer motions and deformations in both normal and tangential directions. Recently developed nanoscale experiments and devices have highlighted that such interactions are often coupled tightly with the physical and mechanical properties of 2D materials, leading to a number of intriguing phenomena that have rarely been observed otherwise. The fundamental understanding of the 2D-2D interactions would help to demystify these phenomena and to explore potential applications.

3.3.1. Strain solitons and moiré superstructures

The classical Frenkel-Kontorova (FK) model has been used to simulate 1D commensurate-incommensurate transitions with a chain of elastically linked atoms in a periodic potential field [157]. The boundaries between commensurate phases can be described in terms of topological defects called solitons, with concentrated chain deformation in the narrow regions. In 2D, the boundaries between commensurate domains are also called domain walls. For bilayer 2D materials, with highly deformable atomic layers interacting with each other in both the normal and shear directions, a slightly incommensurate stacking as a result of relative twist or lattice mismatch may transition to domains of commensurate stacking separated by domain walls or strain solitons [92,158].

For bilayer graphene, the commensurate Bernal stacking (i.e., AB and BA or AC) is most stable with the minimum interlayer potential. When the two graphene layers are not stacked perfectly in the commensurate state, the interlayer potential is higher and can be reduced by forming commensurate domains with alternating AB and BA stacking. The transition from one commensurate stacking to the other can be described as a strain soliton consisting of an atomic-scale

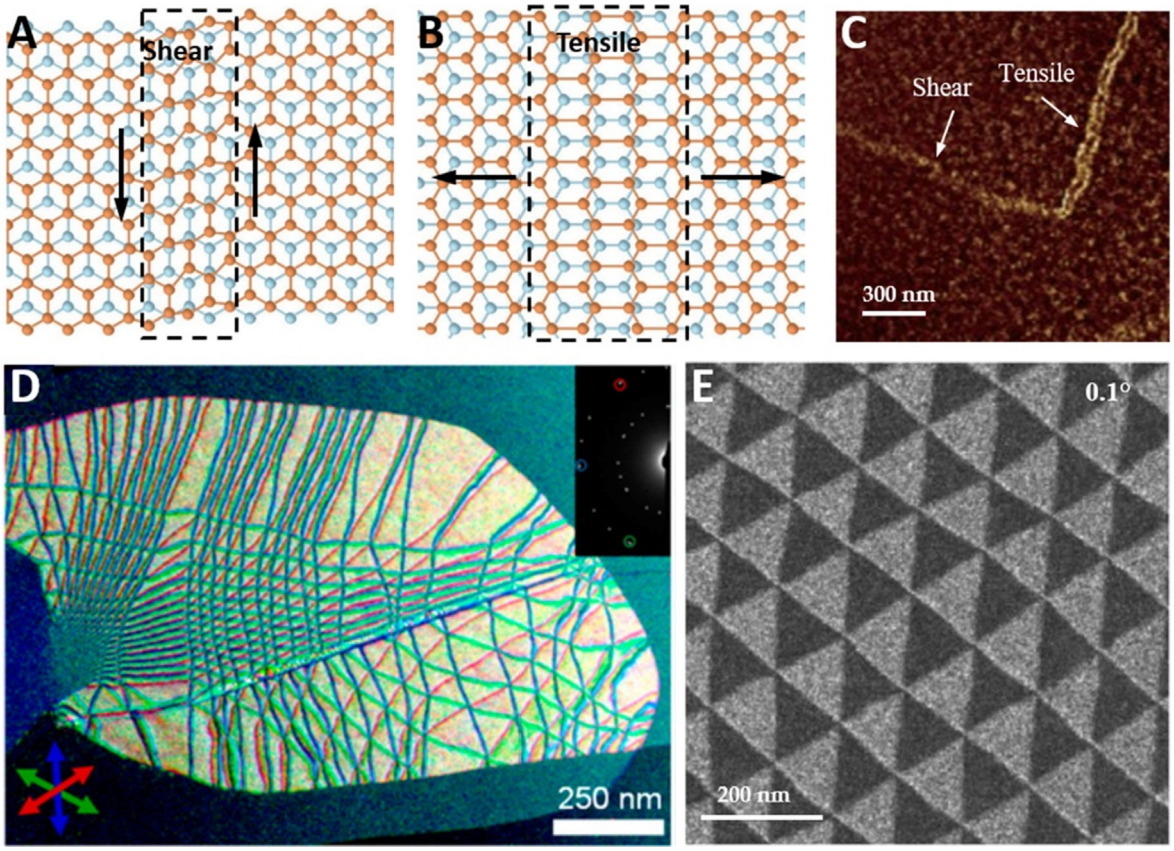

Fig. 8. (**A and B**) Schematic illustrations of a shear and tensile strain solitons. (**C**) Near-field infrared image of an exfoliated bilayer graphene showing an L-shaped domain wall, containing segments of shear and tensile strain solitons distinguishable by different infrared responses. (**A–C**) are adapted with permission from [159]. (**D**) Dark-field TEM image of a CVD-grown bilayer graphene, with three images taken from the [−2 1 1 0] diffraction angles indicated in the inset overlaid in red, blue, and green, where each line is an AB/BA domain wall with its color indicating the direction of relative translation. Figure is adapted with permission from [158]. (**E**) Dark-field TEM image of a twisted bilayer graphene with a controlled twisting angle (0.1°), showing a triangular pattern with alternating contrast of AB/BA domains. Figure is adapted with permission from [160].

registry shift with a translation vector [151,158] or as a partial dislocation with a Burgers vector [161]. Depending on the direction of the translation vector, two types of strain solitons have been identified [158,159]: solitons parallel to the translation vector are characterized by a shear strain, whereas solitons perpendicular to the translation vector are characterized by a tensile strain (Fig. 8A and B). In addition, pronounced out-of-plane deformation of the graphene layers has also been observed [161], which could change the strain state near the solitons and thus impact the electronic properties. A recent study found that the creation and annihilation of individual solitons in bilayer graphene drumhead resonators led to stochastic jumps in frequency [162], suggesting a high electromechanical sensitivity of the 2D resonators to the dynamics of single soliton.

A variety of strain soliton patterns have been observed in bilayer graphene [158,159,161], including triangular and irregular network patterns (Fig. 8D and E), parallel lines, L-shaped (Fig. 8C), and closed loops. Alden et al. [158] found that most of the domain walls in the network pattern (Fig. 8D) were shear strain solitons, resulting from a relative rotation between the two graphene layers. The observed triangular pattern resembles a moiré pattern, but with a key difference in that the graphene lattice has relaxed into locally commensurate phases separated by relatively narrow boundaries (domain walls). Moreover, they noted topological point defects at the intersections of the domain walls, corresponding to AA-stacked graphene (similar to Fig. 7B). They further observed soliton motion during in situ heating above 1000 °C, with topological rearrangements to form more regular patterns [158]. More recently, Yoo et al. [160] reported atomic reconstruction in twisted bilayer graphene and its impact on the electronic properties. They observed a gradual transition from an incommensurate moiré pattern (no relaxation) to a triangular pattern with alternating AB/BA domains (Fig. 8E) as the twist angle decreased across a critical angle ($\approx 1^\circ$). The atomic reconstruction at a small twist angle ($< 1^\circ$) induces significant changes in the lattice symmetry and electronic structure, opening a new pathway to engineering with continuous tunability.

More generally, a periodic 2D moiré pattern forms in bilayer 2D materials with certain degree of incommensurability. For bilayer graphene, the incommensurability may result from a relative twist or differential straining of the two layers. In the case of bilayer heterostructures such as graphene on hBN, the lattice mismatch (~1.8%) between hBN and graphene leads to a hexagonal moiré pattern [14,92,152]. Moreover, depending on the relative twist angle between the two crystals, graphene can either form a partially commensurate state (for small angles) or remains largely incommensurate [92]. In the partially commensurate state, the graphene lattice is stretched to match the underlying hBN lattice in the commensurate areas that are separated by domain walls. With both the lattice mismatch and the relative twist, the domain walls may be described as strain solitons with mixed shear and tensile/compressive strains (relative to the hBN lattice). Similar moiré superstructures have been observed in other bilayer 2D materials and vdW heterostructures [9,163,164], where the interplay between the interlayer mechanical interactions and the intralayer deformation is critical for the commensurate/incommensurate structural transition.

Recently, extensive efforts have been devoted to developing experimental control over the 2D moiré superstructures with unique physical properties by twisting [6,160,165]. The twist angle between

the 2D layers has been exploited to tune the van Hove singularities [166] and to uncover correlated insulating and superconducting states in twisted bilayer graphene [4,5]. It has also allowed to observe the Hofstadter butterfly in graphene on hBN [167]. Moreover, mechanical straining could offer a versatile degree of freedom to control the 2D moiré superstructures, reminiscent of strain engineering [16]. The effect of strain on 2D moiré patterns was notable in a recent work by Zhang et al. [163] where the moiré pattern formed by stacking a lateral WSe_2–MoS_2 heterojunction on top of a monolayer WSe_2 was distorted due to an inhomogeneous strain field. Using scanning tunneling spectroscopy, the distorted 2D moiré pattern was measured to determine the full-field 2D strain tensor with the nanometer resolution [163]. It was found that the lattice-mismatch strain in the lateral WSe_2–MoS_2 heterojunction was partially relieved by dislocations, with a distinctive electronic structure at the interface. Alternatively, each layer in 2D stacks may be strained independently (called heterostrain). Huder et al. [168] showed that a small uniaxial heterostrain in the twisted bilayer graphene, likely due to the pinning of the top layer at its boundaries during growth, could lead to the emergence of flat bands, opening new possibilities for straintronics based on 2D materials. More recently, Edelberg et al. [169] showed that a uniaxial strain led to a commensurate-incommensurate transition in a multilayer $MoSe_2$ system. By straining the bulk $MoSe_2$ substrate, they observed spontaneous formation of topological solitons in the top monolayer, forming a honeycomb-like network pattern, which provided a unique route to achieve deeply confined electron states in a strain-tunable array.

3.3.2. Thermally induced self-rotation and folding

Rich spontaneous mechanical behaviors have been observed in layered vdW materials during thermal annealing, which may be further related to the thermally activated motions of strain solitons [170–172]. For example, Wang et al. [170] reported self-rotation of a monolayer graphene on hBN at a temperature of > 100 °C with a critical twist angle of ~12°, below which graphene tends to rotate towards a relative angle of ~0° (most stable) and above which graphene rotates towards ~30° (metastable). For graphene on hBN, the interplay between the interlayer vdW forces and the intralayer elasticity results in graphene self-rotating towards the stable or metastable crystallographic directions. Such thermally activated self-rotation could be macroscopic for graphene flakes of tens of micrometers with tangential displacement of hundreds of nanometers [171,172], which may be used for manufacturing of aligned vdW heterostructures.

As another example, spontaneous self-tearing and folding of graphene ribbons were observed by Annett and Cross [173] after piercing a graphene layer on a silicon oxide substrate by nanoindentation. They interpreted the observation using a simple fracture mechanics model that highlighted the thermodynamic driving force for formation of the graphene–graphene interface with sufficient strength to overcome the graphene-substrate adhesion and tear the graphene lattice. Such folding could be useful for mechanical metrologies [174–176], vdW structure fabrications [177], 2D material-based origami and composites [178,179]. Extensive efforts have recently focused on how the folding and unfolding of these atomically thin sheets as well as the resulting physical properties can be controlled [124,178,180,181].

3.3.3. Bending with interlayer slip

Interlayer slip between 2D layers has a profound effect on the mechanical properties of multilayer vdW materials. In particular, bending of few-layer graphene (FLG) leads to interlayer slip, and in turn, the interlayer slip lowers the bending stiffness of FLG, according to a recent work by Han et al. [182]. By laying FLG sheets over atomically sharp hBN steps and measuring the bending deformation of FLG by high-resolution cross-sectional imaging, they obtained bending stiffness for FLG up to 12 layers, with values lying between two theoretical limits assuming either zero slip (super-glued) or frictionless (super-lubricated) interlayer slip. Similar results were reported by Wang et al. [183] who measured bending stiffness of multilayered graphene, hBN, and MoS_2 by pressurized blisters. Interestingly, it was found that the bending rigidity of the three types of 2D materials with comparable thickness followed a trend (MoS_2 > hBN > graphene) opposite to their in-plane elastic moduli (MoS_2 < hBN < graphene) [183], likely due to different resistances to the interlayer slip among the three 2D materials. Moreover, Han et al. [182] found that the bending stiffness of FLG depended on the bending angle. Increasing the bending angle led to more interlayer slip between the graphene layers and thus reduced bending stiffness. Therefore, the flexibility of multilayer 2D materials depends on the interlayer slip, and the amount of interlayer slip depends on the bending angle in addition to the interlayer shear strength. Such an intimate coupling could be exploited to achieve highly flexible electronic materials with tunable stiffness.

4. Concluding remarks

This Opinion reviews recent experimental and theoretical studies on the mechanics of 2D material interfaces, including normal (adhesion) and tangential (shear/friction) interactions at the 2D-3D and 2D-2D interfaces. The multiscale nature of the interfaces offers both grand challenges and ample opportunities for future research.

For the 2D-3D interfaces, several experimental methods have been developed to measure the adhesion energy, although significant discrepancies among different measurements remain to be resolved. More insights into the underlying mechanisms of the adhesive interactions can be gained from the interfacial traction-separation relations (TSRs), which however is more challenging to measure, especially for the atomically thin 2D materials. On the theoretical side, understanding remains limited on the underlying interaction mechanisms beyond vdW forces. Further studies are needed to understand the effects of surface roughness and its scale dependence, the rate effect, and the temperature dependence, among others. It is also of practical importance to leverage these effects in designing the interfaces with specific adhesive interactions for applications of the 2D materials in nanocomposites and electronic/photonic devices.

FFM measurements have been used widely for characterizing nanoscale friction of 2D materials, but it is challenging to extract the intrinsic properties of the friction and shear interactions at the 2D-3D interfaces. Alternatively, shear interactions between 2D materials and their 3D substrates have been examined by deforming either the substrates or the 2D materials to induce relative sliding. Further studies are needed to bridge the nanoscale friction by FFM measurements to shear interactions at larger scales.

More generally, the mechanics at the 2D-3D interfaces often involves coupled normal (adhesion) and tangential (friction/shear) interactions, such as the mixed-mode interfacial fracture experiments (e.g., pressurized blister tests) and the FFM experiments. Further studies are needed to unveil the coupling mechanisms and to unify the normal and shear interactions within a general framework of mixed-mode interactions at the 2D-3D interfaces.

For the 2D-2D interfaces, measurements of the interlayer adhesion energy are relatively scarce. In addition to adhesion and separation, where the interlayer vdW forces are predominantly attractions, repulsive interactions between the 2D layers can be activated by compression, leading to an enhanced coupling between the layers with tunable physical and chemical properties. Further studies should consider the interplay between pressure, interlayer registry, and the in-plane and out-of-plane deformations of the 2D layers, with spatially non-uniform, multiscale features (such as strain solitons).

Detailed characterizations on the 2D-2D interlayer friction and shear interactions have been achieved recently, where structural superlubricity has become a common feature between various 2D materials. With more detailed analysis of contact, adhesion and shear interactions in the friction experiments, both the friction coefficient and the shear strength could be determined as the intrinsic properties of the

2D-2D interfaces. Theoretically, registry-dependent interlayer potentials have been developed to model friction and interactions between 2D layers. Recent studies have also considered both in-plane and out-of-plane deformations in 2D bilayers and vdW heterostructures, predicting the formation of peculiar microstructures (e.g., strain solitons and moiré superstructures). Future studies are needed to relate the interfacial microstructures with topological defects to the friction behaviors (stick–slip and superlubricity).

A number of intriguing phenomena have been observed in bilayer 2D materials and vdW heterostructures, resulting from the interplay between the elastic deformation of 2D materials and the unique 2D-2D interactions in both the normal and tangential directions. Future studies are needed to demystify these phenomena based on the fundamental understanding of the 2D-2D interactions and to explore potential applications, including strain engineering of the moiré superstructures in vdW heterostructures.

Declaration of Competing Interest

The authors declare that they have no known competing financial interests or personal relationships that could have appeared to influence the work reported in this paper.

Acknowledgements

Z.D. acknowledges the support by the Graduate Continuing Fellowship from the University of Texas at Austin.

References

[1] A.K. Geim, I.V. Grigorieva, Van der Waals heterostructures, Nature 499 (7459) (2013) 419–425.
[2] Y. Liu, N.O. Weiss, X. Duan, H.-C. Cheng, Y. Huang, X. Duan, Van der Waals heterostructures and devices, Nat. Rev. Mater. 1 (2016) 16042.
[3] K.S. Novoselov, A. Mishchenko, A. Carvalho, A.H. Castro Neto, 2D materials and van der Waals heterostructures, Science 353 (6298) (2016) aac9439.
[4] Y. Cao, V. Fatemi, A. Demir, S. Fang, S.L. Tomarken, J.Y. Luo, J.D. Sanchez-Yamagishi, K. Watanabe, T. Taniguchi, E. Kaxiras, Correlated insulator behaviour at half-filling in magic-angle graphene superlattices, Nature 556 (7699) (2018) 80–84.
[5] Y. Cao, V. Fatemi, S. Fang, K. Watanabe, T. Taniguchi, E. Kaxiras, P. Jarillo-Herrero, Unconventional superconductivity in magic-angle graphene superlattices, Nature 556 (7699) (2018) 43–50.
[6] R. Ribeiro-Palau, C. Zhang, K. Watanabe, T. Taniguchi, J. Hone, C.R. Dean, Twistable electronics with dynamically rotatable heterostructures, Science 361 (6403) (2018) 690–693.
[7] S.S. Sunku, G.X. Ni, B.Y. Jiang, H. Yoo, A. Sternbach, A.S. McLeod, T. Stauber, L. Xiong, T. Taniguchi, K. Watanabe, P. Kim, M.M. Fogler, D.N. Basov, Photonic crystals for nano-light in moire graphene superlattices, Science 362 (6419) (2018) 1153–1156.
[8] M. Yankowitz, S. Chen, H. Polshyn, Y. Zhang, K. Watanabe, T. Taniguchi, D. Graf, A.F. Young, C.R. Dean, Tuning superconductivity in twisted bilayer graphene, Science 363 (6431) (2019) 1059–1064.
[9] C. Jin, E.C. Regan, A. Yan, M. Iqbal Bakti Utama, D. Wang, S. Zhao, Y. Qin, S. Yang, Z. Zheng, S. Shi, K. Watanabe, T. Taniguchi, S. Tongay, A. Zettl, F. Wang, Observation of moire excitons in WSe2/WS2 heterostructure superlattices, Nature 567 (7746) (2019) 76–80.
[10] K.L. Seyler, P. Rivera, H. Yu, N.P. Wilson, E.L. Ray, D.G. Mandrus, J. Yan, W. Yao, X. Xu, Signatures of moire-trapped valley excitons in MoSe2/WSe2 heterobilayers, Nature 567 (7746) (2019) 66–70.
[11] X. Lu, P. Stepanov, W. Yang, M. Xie, M.A. Aamir, I. Das, C. Urgell, K. Watanabe, T. Taniguchi, G. Zhang, A. Bachtold, A.H. MacDonald, D.K. Efetov, Superconductors, orbital magnets and correlated states in magic-angle bilayer graphene, Nature 574 (7780) (2019) 653–657.
[12] K.S. Burch, D. Mandrus, J.G. Park, Magnetism in two-dimensional van der Waals materials, Nature 563 (7729) (2018) 47–52.
[13] M. Yankowitz, J. Jung, E. Laksono, N. Leconte, B.L. Chittari, K. Watanabe, T. Taniguchi, S. Adam, D. Graf, C.R. Dean, Dynamic band-structure tuning of graphene moire superlattices with pressure, Nature 557 (7705) (2018) 404–408.
[14] M. Yankowitz, Q. Ma, P. Jarillo-Herrero, B.J. LeRoy, van der Waals heterostructures combining graphene and hexagonal boron nitride, Nat. Rev. Phys. 1 (2) (2019) 112–125.
[15] D. Akinwande, C.J. Brennan, J.S. Bunch, P. Egberts, J.R. Felts, H. Gao, R. Huang, J.-S. Kim, T. Li, Y. Li, K.M. Liechti, N. Lu, H.S. Park, E.J. Reed, P. Wang, B.I. Yakobson, T. Zhang, Y.-W. Zhang, Y. Zhou, Y. Zhu, A review on mechanics and mechanical properties of 2D materials—Graphene and beyond, Extreme Mech. Lett. 13 (2017) 42–77.
[16] Z. Dai, L. Liu, Z. Zhang, Strain engineering of 2D materials: issues and opportunities at the interface, Adv. Mater. 31 (45) (2019) 1805417.
[17] K.M. Liechti, Characterizing the interfacial behavior of 2D materials: a review, Exp. Mech. 59 (3) (2019) 395–412.
[18] C. Androulidakis, K. Zhang, M. Robertson, S.H. Tawfick, Tailoring the mechanical properties of 2D materials and heterostructures, 2D Mater. 5 (3) (2018) 032005.
[19] S.R. Na, J.W. Suk, R.S. Ruoff, R. Huang, K.M. Liechti, Ultra long-range interactions between large area graphene and silicon, ACS Nano 8 (11) (2014) 11234–11242.
[20] J.W. Suk, S.R. Na, R.J. Stromberg, D. Stauffer, J. Lee, R.S. Ruoff, K.M. Liechti, Probing the adhesion interactions of graphene on silicon oxide by nanoindentation, Carbon 103 (2016) 63–72.
[21] S.P. Koenig, N.G. Boddeti, M.L. Dunn, J.S. Bunch, Ultrastrong adhesion of graphene membranes, Nat. Nanotechnol. 6 (9) (2011) 543–546.
[22] Z. Cao, P. Wang, W. Gao, L. Tao, J. Suk, R. Ruoff, D. Akinwande, R. Huang, K. Liechti, A blister test for interfacial adhesion of large-scale transferred graphene, Carbon 69 (2014) 390–400.
[23] T. Yoon, W.C. Shin, T.Y. Kim, J.H. Mun, T.S. Kim, B.J. Cho, Direct measurement of adhesion energy of monolayer graphene as-grown on copper and its application to renewable transfer process, Nano Lett. 12 (3) (2012) 1448–1452.
[24] Z. Zong, C.-L. Chen, M.R. Dokmeci, K.-T. Wan, Direct measurement of graphene adhesion on silicon surface by intercalation of nanoparticles, J. Appl. Phys. 107 (2010) 026104.
[25] Z. Dai, Y. Hou, D.A. Sanchez, G. Wang, C.J. Brennan, Z. Zhang, L. Liu, N. Lu, Interface-governed deformation of nanobubbles and nanotents formed by two-dimensional materials, Phys. Rev. Lett. 121 (26) (2018) 266101.
[26] C.J. Brennan, J. Nguyen, E.T. Yu, N. Lu, Interface adhesion between 2D materials and elastomers measured by buckle delaminations, Adv. Mater. Interfaces 2 (16) (2015) 1500176.
[27] Z. Dai, G. Wang, L. Liu, Y. Hou, Y. Wei, Z. Zhang, Mechanical behavior and properties of hydrogen bonded graphene/polymer nano-interfaces, Compos. Sci. Technol. 136 (2016) 1–9.
[28] S. Deng, E. Gao, Z. Xu, V. Berry, Adhesion energy of MoS2 thin films on silicon-based substrates determined via the attributes of a single MoS2 wrinkle, ACS Appl. Mater. Interfaces 9 (8) (2017) 7812–7818.
[29] Z. Dai, D.A. Sanchez, C.J. Brennan, N. Lu, Radial buckle delamination around 2D material tents, J. Mech. Phys. Solids 137 (2020) 103843.
[30] D.A. Sanchez, Z. Dai, P. Wang, A. Cantu-Chavez, C.J. Brennan, R. Huang, N. Lu, Mechanics of spontaneously formed nanoblisters trapped by transferred 2D crystals, PNAS 115 (31) (2018) 7884–7889.
[31] T. Jiang, Y. Zhu, Measuring graphene adhesion using atomic force microscopy with a microsphere tip, Nanoscale 7 (24) (2015) 10760–10766.
[32] Y. Li, S. Huang, C. Wei, C. Wu, V.N. Mochalin, Adhesion of two-dimensional titanium carbides (MXenes) and graphene to silicon, Nat. Commun. 10 (2019) 3014.
[33] J. Torres, Y. Zhu, P. Liu, S.C. Lim, M. Yun, Adhesion energies of 2D graphene and MoS2 to silicon and metal substrates, Phys. Status Solidi A 215 (2018) 1700512.
[34] X. Gao, X. Yu, B. Li, S. Fan, C. Li, Measuring graphene adhesion on silicon substrate by single and dual nanoparticle-loaded blister, Adv. Mater. Interfaces 4 (9) (2017) 1601023.
[35] Z. Cao, L. Tao, D. Akinwande, R. Huang, K.M. Liechti, Mixed-mode interactions between graphene and substrates by blister tests, J. Appl. Mech. 82 (8) (2015) 081008.
[36] Z. Cao, L. Tao, D. Akinwande, R. Huang, K.M. Liechti, Mixed-mode traction-separation relations between graphene and copper by blister tests, Int. J. Solids Struct. 84 (2016) 147–159.
[37] H. Xin, R. Borduin, W. Jiang, K.M. Liechti, W. Li, Adhesion energy of as-grown graphene on copper foil with a blister test, Carbon 123 (2017) 243–249.
[38] S.R. Na, J.W. Suk, L. Tao, D. Akinwande, R.S. Ruoff, R. Huang, K.M. Liechti, Selective mechanical transfer of graphene from seed copper foil using rate effects, ACS Nano 9 (2) (2015) 1325–1335.
[39] M.Z. Miskin, C. Sun, I. Cohen, W.R. Dichtel, P.L. McEuen, Measuring and manipulating the adhesion of graphene, Nano Lett. 18 (1) (2018) 449–454.
[40] D. Lloyd, X. Liu, N. Boddeti, L. Cantley, R. Long, M.L. Dunn, J.S. Bunch, Adhesion, stiffness, and instability in atomically thin MoS2 bubbles, Nano Lett. 17 (9) (2017) 5329–5334.
[41] W. Gao, P. Xiao, G. Henkelman, K.M. Liechti, R. Huang, Interfacial adhesion between graphene and silicon dioxide by density functional theory with van der Waals corrections, J. Phys. D Appl. Phys. 47 (25) (2014) 255301.
[42] X. Liu, N.G. Boddeti, M.R. Szpunar, L. Wang, M.A. Rodriguez, R. Long, J. Xiao, M.L. Dunn, J.S. Bunch, Observation of pull-in instability in graphene membranes under interfacial forces, Nano Lett. 13 (5) (2013) 2309–2313.
[43] P. Wang, K.M. Liechti, R. Huang, Snap transitions of pressurized graphene blisters, J. Appl. Mech. 83 (7) (2016) 071002.
[44] C. Xu, T. Yang, Y. Kang, Q. Li, T. Xue, K.M. Liechti, R. Huang, W. Qiu, Rate-dependent decohesion modes in graphene-sandwiched interfaces, Adv. Mater. Interfaces 6 (23) (2019) 1901217.
[45] W. Gao, K.M. Liechti, R. Huang, Wet adhesion of graphene, Extreme Mech. Lett. 3 (2015) 130–140.
[46] S. Kumar, D. Parks, K. Kamrin, Mechanistic origin of the Ultrastrong adhesion between graphene and a-SiO2: beyond van der Waals, ACS Nano 10 (7) (2016) 6552–6562.
[47] W. Gao, R. Huang, Effect of surface roughness on adhesion of graphene membranes, J. Phys. D Appl. Phys. 44 (45) (2011) 452001.
[48] J.S. Bunch, M.L. Dunn, Adhesion mechanics of graphene membranes, Solid State Commun. 152 (15) (2012) 1359–1364.
[49] W. Chang, S. Rajan, B. Peng, C. Ren, M. Sutton, C. Li, Adhesion energy of as-grown

graphene on nickel substrates via StereoDIC based blister experiments, Carbon 153 (2019) 699–706.
[50] S.R. Na, N. Rahimi, L. Tao, H. Chou, S.K. Ameri, D. Akinwande, K. Liechti, Clean graphene interfaces by selective dry transfer for large area silicon integration, Nanoscale 8 (2016) 7523–7533.
[51] S.R. Na, S. Rahimi, L. Tao, H. Chou, S.K. Ameri, D. Akinwande, K.M. Liechti, Clean graphene interfaces by selective dry transfer for large area silicon integration, Nanoscale 8 (14) (2016) 7523–7533.
[52] Y. Wei, A stochastic description on the traction-separation law of an interface with non-covalent bonding, J. Mech. Phys. Solids 70 (2014) 227–241.
[53] J. Qian, J. Lin, G.-K. Xu, Y. Lin, H. Gao, Thermally assisted peeling of an elastic strip in adhesion with a substrate via molecular bonds, J. Mech. Phys. Solids 101 (2017) 197–208.
[54] T. Yang, X. Yang, R. Huang, K.M. Liechti, Rate-dependent traction-separation relations for a silicon/epoxy interface informed by experiments and bond rupture kinetics, J. Mech. Phys. Solids 131 (2019) 1–19.
[55] W. Gao, R. Huang, Thermomechanics of monolayer graphene: Rippling, thermal expansion and elasticity, J. Mech. Phys. Solids 66 (2014) 42–58.
[56] A. Košmrlj, D.R. Nelson, Response of thermalized ribbons to pulling and bending, Phys. Rev. B 93 (12) (2016) 125431.
[57] P. Wang, W. Gao, R. Huang, Entropic effects of thermal rippling on van der Waals interactions between monolayer graphene and a rigid substrate, J. Appl. Phys. 119 (7) (2016) 074305.
[58] Z. Chang, R. Yang, Y. Wei, The linear-dependence of adhesion strength and adhesion range on temperature in soft membranes, J. Mech. Phys. Solids 132 (2019) 103697.
[59] T. Filleter, J.L. McChesney, A. Bostwick, E. Rotenberg, K.V. Emtsev, T. Seyller, K. Horn, R. Bennewitz, Friction and dissipation in epitaxial graphene films, Phys. Rev. Lett. 102 (8) (2009) 086102.
[60] C. Lee, Q. Li, W. Kalb, X.Z. Liu, H. Berger, R.W. Carpick, J. Hone, Frictional characteristics of atomically thin sheets, Science 328 (5974) (2010) 76–80.
[61] Z. Deng, A. Smolyanitsky, Q. Li, X.-Q. Feng, R.J. Cannara, Adhesion-dependent negative friction coefficient on chemically modified graphite at the nanoscale, Nat. Mater. 11 (12) (2012) 1032–1037.
[62] P. Egberts, G.H. Han, X.Z. Liu, A.T. Johnson, R.W. Carpick, Frictional behavior of atomically thin sheets: hexagonal-shaped graphene islands grown on copper by chemical vapor deposition, ACS Nano 8 (5) (2014) 5010–5021.
[63] S. Zhang, T. Ma, A. Erdemir, Q. Li, Tribology of two-dimensional materials: From mechanisms to modulating strategies, Mater. Today 26 (2019) 67–86.
[64] L. Gong, I.A. Kinloch, R.J. Young, I. Riaz, R. Jalil, K.S. Novoselov, Interfacial stress transfer in a graphene monolayer nanocomposite, Adv. Mater. 22 (24) (2010) 2694–2697.
[65] T. Jiang, R. Huang, Y. Zhu, Interfacial sliding and buckling of monolayer graphene on a stretchable substrate, Adv. Funct. Mater. 24 (3) (2014) 396–402.
[66] C. Xu, T. Xue, W. Qiu, Y. Kang, Size effect of the interfacial mechanical behavior of graphene on a stretchable substrate, ACS Appl. Mater. Interfaces 8 (40) (2016) 27099–27106.
[67] G. Wang, Z. Dai, L. Liu, H. Hu, Q. Dai, Z. Zhang, Tuning the interfacial mechanical behaviors of monolayer graphene/PMMA nanocomposites, ACS Appl. Mater. Interfaces 8 (34) (2016) 22554–22562.
[68] S.R. Na, X. Wang, R.D. Piner, R. Huang, C.G. Willson, K.M. Liechti, Cracking of polycrystalline graphene on copper under tension, ACS Nano 10 (10) (2016) 9616–9625.
[69] S. Kawai, A. Benassi, E. Gnecco, H. Sode, R. Pawlak, X. Feng, K. Mullen, D. Passerone, C.A. Pignedoli, P. Ruffieux, R. Fasel, E. Meyer, Superlubricity of graphene nanoribbons on gold surfaces, Science 351 (6276) (2016) 957–961.
[70] A.L. Kitt, Z. Qi, S. Rémi, H.S. Park, A.K. Swan, B.B. Goldberg, How graphene slides: Measurement and theory of strain-dependent frictional forces between graphene and SiO2, Nano Lett. 13 (6) (2013) 2605–2610.
[71] G. Wang, Z. Dai, Y. Wang, P. Tan, L. Liu, Z. Xu, Y. Wei, R. Huang, Z. Zhang, Measuring interlayer shear stress in bilayer graphene, Phys. Rev. Lett. 119 (3) (2017) 036101.
[72] S. Li, Q. Li, R.W. Carpick, P. Gumbsch, X.Z. Liu, X. Ding, J. Sun, J. Li, The evolving quality of frictional contact with graphene, Nature 539 (7630) (2016) 541–545.
[73] Y. Dong, Effects of substrate roughness and electron–phonon coupling on thickness-dependent friction of graphene, J. Phys. D Appl. Phys. 47 (5) (2014) 055305.
[74] A. Smolyanitsky, J.P. Killgore, V.K. Tewary, Effect of elastic deformation on frictional properties of few-layer graphene, Phys. Rev. B 85 (3) (2012) 035412.
[75] A. Smolyanitsky, S. Zhu, Z. Deng, T. Li, R.J. Cannara, Effects of surface compliance and relaxation on the frictional properties of lamellar materials, RSC Adv. 4 (51) (2014) 26721–26728.
[76] X.-Y. Sun, Y.-Z. Qi, W. Ouyang, X.-Q. Feng, Q. Li, Energy corrugation in atomic-scale friction on graphite revisited by molecular dynamics simulations, Acta Mech. Sinica 32 (4) (2016) 604–610.
[77] S. Kwon, J.H. Ko, K.J. Jeon, Y.H. Kim, J.Y. Park, Enhanced nanoscale friction on fluorinated graphene, Nano Lett. 12 (12) (2012) 6043–6048.
[78] J.-H. Ko, S. Kwon, I.-S. Byun, J.S. Choi, B.H. Park, Y.-H. Kim, J.Y. Park, Nanotribological properties of fluorinated, hydrogenated, and oxidized graphenes, Tribol. Lett. 50 (2) (2013) 137–144.
[79] Q. Li, X.-Z. Liu, S.-P. Kim, V.B. Shenoy, P.E. Sheehan, J.T. Robinson, R.W. Carpick, Fluorination of graphene enhances friction due to increased corrugation, Nano Lett. 14 (9) (2014) 5212–5217.
[80] H. Chen, T. Filleter, Effect of structure on the tribology of ultrathin graphene and graphene oxide films, Nanotechnology 26 (13) (2015) 135702.
[81] M. Daly, C. Cao, H. Sun, Y. Sun, T. Filleter, C.V. Singh, Interfacial shear strength of multilayer graphene oxide films, ACS Nano 10 (2) (2016) 1939–1947.
[82] L.-F. Wang, T.-B. Ma, Y.-Z. Hu, H. Wang, T.-M. Shao, Ab initio study of the friction mechanism of fluorographene and graphane, J. Phys. Chem. C 117 (24) (2013) 12520–12525.
[83] Y. Dong, X. Wu, A. Martini, Atomic roughness enhanced friction on hydrogenated graphene, Nanotechnology 24 (37) (2013) 375701.
[84] T.D. Jacobs, R.W. Carpick, Nanoscale wear as a stress-assisted chemical reaction, Nat. Nanotechnol. 8 (2) (2013) 108–112.
[85] V. Vahdat, D.S. Grierson, K.T. Turner, R.W. Carpick, Mechanics of interaction and atomic-scale wear of amplitude modulation atomic force microscopy probes, ACS Nano 7 (4) (2013) 3221–3235.
[86] J.R. Felts, A.J. Oyer, S.C. Hernandez, K.E. Whitener Jr., J.T. Robinson, S.G. Walton, P.E. Sheehan, Direct mechanochemical cleavage of functional groups from graphene, Nat. Commun. 6 (2015) 6467.
[87] G. Paolicelli, M. Tripathi, V. Corradini, A. Candini, S. Valeri, Nanoscale frictional behavior of graphene on SiO2 and Ni (111) substrates, Nanotechnology 26 (5) (2015) 055703.
[88] Z. Ye, P. Egberts, G.H. Han, A.T. Johnson, R.W. Carpick, A. Martini, Load-dependent friction hysteresis on graphene, ACS Nano 10 (5) (2016) 5161–5168.
[89] P. Gong, Z. Ye, L. Yuan, P. Egberts, Evaluation of wetting transparency and surface energy of pristine and aged graphene through nanoscale friction, Carbon 132 (2018) 749–759.
[90] D.-H. Cho, L. Wang, J.-S. Kim, G.-H. Lee, E.S. Kim, S. Lee, S.Y. Lee, J. Hone, C. Lee, Effect of surface morphology on friction of graphene on various substrates, Nanoscale 5 (7) (2013) 3063–3069.
[91] M.B. Elinski, Z. Liu, J.C. Spear, J.D. Batteas, 2D or not 2D? The impact of nanoscale roughness and substrate interactions on the tribological properties of graphene and MoS2, J. Phys. D Appl. Phys. 50 (10) (2017) 103003.
[92] C. Woods, L. Britnell, A. Eckmann, R. Ma, J. Lu, H. Guo, X. Lin, G. Yu, Y. Cao, R. Gorbachev, Commensurate-incommensurate transition in graphene on hexagonal boron nitride, Nat. Phys. 10 (6) (2014) 451–456.
[93] X. Zheng, L. Gao, Q. Yao, Q. Li, M. Zhang, X. Xie, S. Qiao, G. Wang, T. Ma, Z. Di, J. Luo, X. Wang, Robust ultra-low-friction state of graphene via moire superlattice confinement, Nat. Commun. 7 (2016) 13204.
[94] N. Chan, S. Balakrishna, A. Klemenz, M. Moseler, P. Egberts, R. Bennewitz, Contrast in nanoscale friction between rotational domains of graphene on Pt (111), Carbon 113 (2017) 132–138.
[95] J. Liu, S. Zhang, Q. Li, X.-Q. Feng, Z. Di, C. Ye, Y. Dong, Lateral force modulation by moiré superlattice structure: Surfing on periodically undulated graphene sheets, Carbon 125 (2017) 76–83.
[96] X. Zeng, Y. Peng, H. Lang, A novel approach to decrease friction of graphene, Carbon 118 (2017) 233–240.
[97] J.C. Spear, J.P. Custer, J.D. Batteas, The influence of nanoscale roughness and substrate chemistry on the frictional properties of single and few layer graphene, Nanoscale 7 (22) (2015) 10021–10029.
[98] Z. Deng, N.N. Klimov, S.D. Solares, T. Li, H. Xu, R.J. Cannara, Nanoscale interfacial friction and adhesion on supported versus suspended monolayer and multilayer graphene, Langmuir 29 (1) (2013) 235–243.
[99] J.D. Wood, C.M. Harvey, S. Wang, Adhesion toughness of multilayer graphene films, Nat. Commun. 8 (2017) 1952.
[100] J.W. Hutchinson, Z. Suo, Mixed mode cracking in layered materials, Adv. Appl. Mech. 29 (1991) 63–191.
[101] A.G. Evans, J.W. Hutchinson, Effects of non-planarity on the mixed mode fracture resistance of bimaterial interfaces, Acta Metall. 37 (3) (1989) 909–916.
[102] D.L. Duong, S.J. Yun, Y.H. Lee, van der Waals layered materials: opportunities and challenges, ACS Nano 11 (12) (2017) 11803–11830.
[103] Z. Liu, J.Z. Liu, Y. Cheng, Z. Li, L. Wang, Q. Zheng, Interlayer binding energy of graphite: A mesoscopic determination from deformation, Phys. Rev. B 85 (20) (2012) 205418.
[104] W. Wang, S. Dai, X. Li, J. Yang, D.J. Srolovitz, Q. Zheng, Measurement of the cleavage energy of graphite, Nat. Commun. 6 (2015) 7853.
[105] E. Koren, E. Lortscher, C. Rawlings, A.W. Knoll, U. Duerig, Surface science. Adhesion and friction in mesoscopic graphite contacts, Science 348 (6235) (2015) 679–683.
[106] E. Khestanova, F. Guinea, L. Fumagalli, A.K. Geim, I.V. Grigorieva, Universal shape and pressure inside bubbles appearing in van der Waals heterostructures, Nat. Commun. 7 (2016) 12587.
[107] F. Pizzocchero, L. Gammelgaard, B.S. Jessen, J.M. Caridad, L. Wang, J. Hone, P. Boggild, T.J. Booth, The hot pick-up technique for batch assembly of van der Waals heterostructures, Nat. Commun. 7 (2016) 11894.
[108] D.G. Purdie, N.M. Pugno, T. Taniguchi, K. Watanabe, A.C. Ferrari, A. Lombardo, Cleaning interfaces in layered materials heterostructures, Nat. Commun. 9 (2018) 5387.
[109] J. Wang, D.C. Sorescu, S. Jeon, A. Belianinov, S.V. Kalinin, A.P. Baddorf, P. Maksymovych, Atomic intercalation to measure adhesion of graphene on graphite, Nat. Commun. 7 (2016) 13263.
[110] P. Wang, W. Gao, Z. Cao, K.M. Liechti, R. Huang, Numerical analysis of circular graphene bubbles, J. Appl. Mech. 80 (4) (2013) 040905.
[111] K. Yue, W. Gao, R. Huang, K.M. Liechti, Analytical methods for the mechanics of graphene bubbles, J. Appl. Phys. 112 (8) (2012) 083512.
[112] B. Li, J. Yin, X. Liu, H. Wu, J. Li, X. Li, W. Guo, Probing van der Waals interactions at two-dimensional heterointerfaces, Nat. Nanotechnol. 14 (6) (2019) 567–572.
[113] R. Frisenda, E. Navarro-Moratalla, P. Gant, D. Perez De Lara, P. Jarillo-Herrero, R.V. Gorbachev, A. Castellanos-Gomez, Recent progress in the assembly of nanodevices and van der Waals heterostructures by deterministic placement of 2D materials, Chem. Soc. Rev. 47 (1) (2018) 53–68.
[114] A. Castellanos-Gomez, M. Buscema, R. Molenaar, V. Singh, L. Janssen, H.S. Van

Der Zant, G.A. Steele, Deterministic transfer of two-dimensional materials by all-dry viscoelastic stamping, 2D Mater. 1 (1) (2014) 011002.
[115] S.J. Haigh, A. Gholinia, R. Jalil, S. Romani, L. Britnell, D.C. Elias, K.S. Novoselov, L.A. Ponomarenko, A.K. Geim, R. Gorbachev, Cross-sectional imaging of individual layers and buried interfaces of graphene-based heterostructures and superlattices, Nat. Mater. 11 (9) (2012) 764–767.
[116] T. Uwanno, Y. Hattori, T. Taniguchi, K. Watanabe, K. Nagashio, Fully dry PMMA transfer of graphene on h-BN using a heating/cooling system, 2D Mater. 2 (4) (2015) 041002.
[117] M.R. Rosenberger, H.J. Chuang, K.M. McCreary, A.T. Hanbicki, S.V. Sivaram, B.T. Jonker, Nano-"Squeegee" for the creation of clean 2D material interfaces, ACS Appl. Mater. Interfaces 10 (12) (2018) 10379–10387.
[118] Y. Gao, T. Cao, F. Cellini, C. Berger, W.A. de Heer, E. Tosatti, E. Riedo, A. Bongiorno, Ultrahard carbon film from epitaxial two-layer graphene, Nat. Nanotechnol. 13 (2) (2018) 133–138.
[119] P.K. Nayak, Y. Horbatenko, S. Ahn, G. Kim, J.-U. Lee, K.Y. Ma, A.-R. Jang, H. Lim, D. Kim, S. Ryu, Probing evolution of twist-angle-dependent interlayer excitons in MoSe2/WSe2 van der Waals heterostructures, ACS Nano 11 (4) (2017) 4041–4050.
[120] T. Li, S. Jiang, N. Sivadas, Z. Wang, Y. Xu, D. Weber, J.E. Goldberger, K. Watanabe, T. Taniguchi, C.J. Fennie, K. Fai Mak, J. Shan, Pressure-controlled interlayer magnetism in atomically thin CrI3, Nat. Mater. 18 (12) (2019) 1303–1308.
[121] T. Song, Z. Fei, M. Yankowitz, Z. Lin, Q. Jiang, K. Hwangbo, Q. Zhang, B. Sun, T. Taniguchi, K. Watanabe, M.A. McGuire, D. Graf, T. Cao, J.H. Chu, D.H. Cobden, C.R. Dean, D. Xiao, X. Xu, Switching 2D magnetic states via pressure tuning of layer stacking, Nat. Mater. 18 (12) (2019) 1298–1302.
[122] Y. Gao, S. Kim, S. Zhou, H.-C. Chiu, D. Nélias, C. Berger, W. De Heer, L. Polloni, R. Sordan, A. Bongiorno, Elastic coupling between layers in two-dimensional materials, Nat. Mater. 14 (7) (2015) 714–720.
[123] M. Yankowitz, K. Watanabe, T. Taniguchi, P. San-Jose, B.J. LeRoy, Pressure-induced commensurate stacking of graphene on boron nitride, Nat. Commun. 7 (2016) 13168.
[124] H. Chen, X.L. Zhang, Y.Y. Zhang, D. Wang, D.L. Bao, Y. Que, W. Xiao, S. Du, M. Ouyang, S.T. Pantelides, H.J. Gao, Atomically precise, custom-design origami graphene nanostructures, Science 365 (6457) (2019) 1036–1040.
[125] O. Hod, E. Meyer, Q. Zheng, M. Urbakh, Structural superlubricity and ultralow friction across the length scales, Nature 563 (7732) (2018) 485–492.
[126] K. Miura, S. Kamiya, Observation of the Amontons-Coulomb law on the nanoscale: frictional forces between MoS2 flakes and MoS2 surfaces, EPL 58 (4) (2002) 610–615.
[127] K. Miura, N. Sasaki, S. Kamiya, Friction mechanisms of graphite from a single-atomic tip to a large-area flake tip, Phys. Rev. B 69 (7) (2004) 075420.
[128] M. Dienwiebel, G.S. Verhoeven, N. Pradeep, J.W. Frenken, J.A. Heimberg, H.W. Zandbergen, Superlubricity of graphite, Phys. Rev. Lett. 92 (12) (2004) 126101.
[129] M. Hirano, K. Shinjo, Atomistic locking and friction, Phys. Rev. B 41 (17) (1990) 11837–11851.
[130] K.M. Liechti, Materials science. Understanding friction in layered materials, Science 348 (6235) (2015) 632–633.
[131] Z. Liu, J. Yang, F. Grey, J.Z. Liu, Y. Liu, Y. Wang, Y. Yang, Y. Cheng, Q. Zheng, Observation of microscale superlubricity in graphite, Phys. Rev. Lett. 108 (20) (2012) 205503.
[132] H. Li, J. Wang, S. Gao, Q. Chen, L. Peng, K. Liu, X. Wei, Superlubricity between MoS2 Monolayers, Adv. Mater. 29 (2017) 1701474.
[133] J.P. Oviedo, S. Kc, N. Lu, J. Wang, K. Cho, R.M. Wallace, M.J. Kim, In situ TEM characterization of shear-stress-induced interlayer sliding in the cross section view of molybdenum disulfide, ACS Nano 9 (2) (2015) 1543–1551.
[134] Y. Song, D. Mandelli, O. Hod, M. Urbakh, M. Ma, Q. Zheng, Robust microscale superlubricity in graphite/hexagonal boron nitride layered heterojunctions, Nat. Mater. 17 (10) (2018) 894–899.
[135] H. Büch, A. Rossi, S. Forti, D. Convertino, V. Tozzini, C. Coletti, Superlubricity of epitaxial monolayer WS 2 on graphene, Nano Res. 11 (11) (2018) 5946–5956.
[136] Y. Kobayashi, T. Taniguchi, K. Watanabe, Y. Maniwa, Y. Miyata, Slidable atomic layers in van der Waals heterostructures, Appl. Phys Express 10 (4) (2017) 045201.
[137] Y. Liu, A. Song, Z. Xu, R. Zong, J. Zhang, W. Yang, R. Wang, Y. Hu, J. Luo, T. Ma, Interlayer friction and superlubricity in single-crystalline contact enabled by two-dimensional flake-wrapped atomic force microscope tips, ACS Nano 12 (8) (2018) 7638–7646.
[138] S.W. Liu, H.P. Wang, Q. Xu, T.B. Ma, G. Yu, C. Zhang, D. Geng, Z. Yu, S. Zhang, W. Wang, Y.Z. Hu, H. Wang, J. Luo, Robust microscale superlubricity under high contact pressure enabled by graphene-coated microsphere, Nat. Commun. 8 (2017) 14029.
[139] A. Kis, K. Jensen, S. Aloni, W. Mickelson, A. Zettl, Interlayer forces and ultralow sliding friction in multiwalled carbon nanotubes, Phys. Rev. Lett. 97 (2) (2006) 025501.
[140] I. Singer, R. Bolster, J. Wegand, S. Fayeulle, B. Stupp, Hertzian stress contribution to low friction behavior of thin MoS2 coatings, Appl. Phys. Lett. 57 (10) (1990) 995–997.
[141] A. Vanossi, N. Manini, M. Urbakh, S. Zapperi, E. Tosatti, Colloquium: Modeling friction: From nanoscale to mesoscale, Rev. Mod. Phys. 85 (2) (2013) 529–552.
[142] G.S. Verhoeven, M. Dienwiebel, J.W. Frenken, Model calculations of superlubricity of graphite, Phys. Rev. B 70 (16) (2004) 165418.
[143] K. Matsushita, H. Matsukawa, N. Sasaki, Atomic scale friction between clean graphite surfaces, Solid State Commun. 136 (1) (2005) 51–55.
[144] A.N. Kolmogorov, V.H. Crespi, Registry-dependent interlayer potential for graphitic systems, Phys. Rev. B 71 (23) (2005) 235415.
[145] K. Zhang, E.B. Tadmor, Structural and electron diffraction scaling of twisted graphene bilayers, J. Mech. Phys. Solids 112 (2018) 225–238.
[146] K. Zhang, E.B. Tadmor, Energy and moiré patterns in 2D bilayers in translation and rotation: A study using an efficient discrete–continuum interlayer potential, Extreme Mech. Lett. 14 (2017) 16–22.
[147] E. Koren, U. Duerig, Superlubricity in quasicrystalline twisted bilayer graphene, Phys. Rev. B 93 (20) (2016) 201404.
[148] Y. Guo, W. Guo, C. Chen, Modifying atomic-scale friction between two graphene sheets: A molecular-force-field study, Phys. Rev. B 76 (15) (2007) 155429.
[149] I. Leven, T. Maaravi, I. Azuri, L. Kronik, O. Hod, Interlayer Potential for Graphene/h-BN Heterostructures, J. Chem. Theory Comput. 12 (6) (2016) 2896–2905.
[150] T. Maaravi, I. Leven, I. Azuri, L. Kronik, O. Hod, Interlayer potential for homogeneous graphene and hexagonal boron nitride systems: reparametrization for many-body dispersion effects, J. Phys. Chem. C 121 (41) (2017) 22826–22835.
[151] H. Kumar, L. Dong, V.B. Shenoy, Limits of coherency and strain transfer in flexible 2D van der Waals heterostructures: formation of strain solitons and interlayer debonding, Sci. Rep. 6 (2016) 21516.
[152] D. Mandelli, W. Ouyang, O. Hod, M. Urbakh, Negative friction coefficients in superlubric graphite-hexagonal boron nitride heterojunctions, Phys. Rev. Lett. 122 (7) (2019) 076102.
[153] T. Gyalog, H. Thomas, Friction between atomically flat surfaces, EPL 37 (3) (1997) 195–200.
[154] H. Kumar, D. Er, L. Dong, J. Li, V.B. Shenoy, Elastic deformations in 2D van der waals heterostructures and their impact on optoelectronic properties: predictions from a multiscale computational approach, Sci. Rep. 5 (2015) 10872.
[155] D. Mandelli, I. Leven, O. Hod, M. Urbakh, Sliding friction of graphene/hexagonal–boron nitride heterojunctions: a route to robust superlubricity, Sci. Rep. 7 (2017) 10851.
[156] W. Ouyang, D. Mandelli, M. Urbakh, O. Hod, Nanoserpents: graphene nanoribbons motion on two-dimensional hexagonal materials, Nano Lett. 18 (9) (2018) 6009–6016.
[157] O.M. Braun, Y.S. Kivshar, The Frenkel-Kontorova Model: Concepts, Methods, and Applications, Springer Science & Business Media, 2013.
[158] J.S. Alden, A.W. Tsen, P.Y. Huang, R. Hovden, L. Brown, J. Park, D.A. Muller, P.L. McEuen, Strain solitons and topological defects in bilayer graphene, Proc. Natl. Acad. Sci. 110 (28) (2013) 11256–11260.
[159] L. Jiang, Z. Shi, B. Zeng, S. Wang, J.-H. Kang, T. Joshi, C. Jin, L. Ju, J. Kim, T. Lyu, Soliton-dependent plasmon reflection at bilayer graphene domain walls, Nat. Mater. 15 (8) (2016) 840–844.
[160] H. Yoo, R. Engelke, S. Carr, S. Fang, K. Zhang, P. Cazeaux, S.H. Sung, R. Hovden, A.W. Tsen, T. Taniguchi, K. Watanabe, G.C. Yi, M. Kim, M. Luskin, E.B. Tadmor, E. Kaxiras, P. Kim, Atomic and electronic reconstruction at the van der Waals interface in twisted bilayer graphene, Nat. Mater. 18 (5) (2019) 448–453.
[161] B. Butz, C. Dolle, F. Niekiel, K. Weber, D. Waldmann, H.B. Weber, B. Meyer, E. Spiecker, Dislocations in bilayer graphene, Nature 505 (7484) (2014) 533–537.
[162] S. Kim, E. Annevelink, E. Han, J. Yu, P.Y. Huang, E. Ertekin, A.M. van der Zande, Stochastic stress jumps due to soliton dynamics in two-dimensional van der Waals interfaces, Nano Lett. 20 (2) (2020) 1201–1207.
[163] C. Zhang, M.-Y. Li, J. Tersoff, Y. Han, Y. Su, L.-J. Li, D.A. Muller, C.-K. Shih, Strain distributions and their influence on electronic structures of WSe 2–MoS 2 laterally strained heterojunctions, Nat. Nanotechnol. 13 (2018) 152–158.
[164] L. McGilly, A. Kerelsky, N. Finney, K. Shapovalov, E.-M. Shih, A. Ghiotto, Y. Zeng, S. Moore, W. Wu, Y. Bai, K. Watanabe, T. Taniguchi, M. Stengel, L. Zhou, J. Hone, X. Zhu, D.N. Basov, C. Dean, C.E. Dreyer, A.N. Pasupathy, Visualization of moiré superlattices, Nat. Nanotechnol. 15 (2020) 580–584.
[165] E. Koren, I. Leven, E. Lörtscher, A. Knoll, O. Hod, U. Duerig, Coherent commensurate electronic states at the interface between misoriented graphene layers, Nat. Nanotechnol. 11 (9) (2016) 752–757.
[166] G. Li, A. Luican, J.L. Dos Santos, A.C. Neto, A. Reina, J. Kong, E. Andrei, Observation of Van Hove singularities in twisted graphene layers, Nat. Phys. 6 (2) (2010) 109–113.
[167] C.R. Dean, L. Wang, P. Maher, C. Forsythe, F. Ghahari, Y. Gao, J. Katoch, M. Ishigami, P. Moon, M. Koshino, T. Taniguchi, K. Watanabe, K.L. Shepard, J. Hone, P. Kim, Hofstadter's butterfly and the fractal quantum Hall effect in moire superlattices, Nature 497 (7451) (2013) 598–602.
[168] L. Huder, A. Artaud, T. Le Quang, G.T. de Laissardiere, A.G.M. Jansen, G. Lapertot, C. Chapelier, V.T. Renard, Electronic spectrum of twisted graphene layers under heterostrain, Phys. Rev. Lett. 120 (15) (2018) 156405.
[169] D. Edelberg, H. Kumar, V. Shenoy, H. Ochoa, A.N. Pasupathy, Tunable strain soliton networks confine electrons in van der Waals materials, Nat. Phys. (2020), https://doi.org/10.1038/s41567-020-0953-2.
[170] D. Wang, G. Chen, C. Li, M. Cheng, W. Yang, S. Wu, G. Xie, J. Zhang, J. Zhao, X. Lu, P. Chen, G. Wang, J. Meng, J. Tang, R. Yang, C. He, D. Liu, D. Shi, K. Watanabe, T. Taniguchi, J. Feng, Y. Zhang, G. Zhang, Thermally induced graphene rotation on hexagonal boron nitride, Phys. Rev. Lett. 116 (12) (2016) 126101.
[171] C.R. Woods, F. Withers, M.J. Zhu, Y. Cao, G. Yu, A. Kozikov, M. Ben Shalom, S.V. Morozov, M.M. van Wijk, A. Fasolino, M.I. Katsnelson, K. Watanabe, T. Taniguchi, A.K. Geim, A. Mishchenko, K.S. Novoselov, Macroscopic self-reorientation of interacting two-dimensional crystals, Nat. Commun. 7 (2016) 10800.
[172] L. Wang, Y. Gao, B. Wen, Z. Han, T. Taniguchi, K. Watanabe, M. Koshino, J. Hone, C.R. Dean, Evidence for a fractional fractal quantum Hall effect in graphene superlattices, Science 350 (6265) (2015) 1231–1234.
[173] J. Annett, G.L. Cross, Self-assembly of graphene ribbons by spontaneous self-tearing and peeling from a substrate, Nature 535 (7611) (2016) 271–275.

[174] W. Qu, S. Bagchi, X. Chen, H.B. Chew, C. Ke, Bending and interlayer shear moduli of ultrathin boron nitride nanosheet, J. Phys. D Appl. Phys. 52 (46) (2019) 465301.
[175] X. Chen, C. Yi, C. Ke, Bending stiffness and interlayer shear modulus of few-layer graphene, Appl. Phys. Lett. 106 (10) (2015) 101907.
[176] J. Zhao, Q. Deng, T.H. Ly, G.H. Han, G. Sandeep, M.H. Rümmeli, Two-dimensional membrane as elastic shell with proof on the folds revealed by three-dimensional atomic mapping, Nat. Commun. 6 (2015) 8935.
[177] J.C. Rode, D. Zhai, C. Belke, S.J. Hong, H. Schmidt, N. Sandler, R.J. Haug, Linking interlayer twist angle to geometrical parameters of self-assembled folded graphene structures, 2D Mater. 6 (2018) 015021.
[178] K. Akius, J. van Ruitenbeek, Graphene nano-origami using Scanning Tunneling Microscopy, arXiv preprint arXiv:1812.09501 (2018).
[179] B. Wang, B.V. Cunning, N.Y. Kim, F. Kargar, S.Y. Park, Z. Li, S.R. Joshi, L. Peng, V. Modepalli, X. Chen, Y. Shen, W.K. Seong, Y. Kwon, J. Jang, H. Shi, C. Gao, G.H. Kim, T.J. Shin, K. Kim, J.Y. Kim, A.A. Balandin, Z. Lee, R.S. Ruoff, Ultrastiff, strong, and highly thermally conductive crystalline graphitic films with mixed stacking order, Adv. Mater. 31 (2019) 1903039.
[180] B. Wang, M. Huang, N.Y. Kim, B.V. Cunning, Y. Huang, D. Qu, X. Chen, S. Jin, M. Biswal, X. Zhang, S.H. Lee, H. Lim, W.J. Yoo, Z. Lee, R.S. Ruoff, Controlled folding of single crystal graphene, Nano Lett. 17 (3) (2017) 1467–1473.
[181] C.L. Yi, L.Y. Zhang, X.M. Chen, X.Q. Wang, C.H. Ke, Nanomechanical unfolding of self-folded graphene on flat substrate, Exp. Mech. 59 (3) (2019) 381–386.
[182] E. Han, J. Yu, E. Annevelink, J. Son, D.A. Kang, K. Watanabe, T. Taniguchi, E. Ertekin, P.Y. Huang, A.M. van der Zande, Ultrasoft slip-mediated bending in few-layer graphene, Nat. Mater. 19 (3) (2020) 305–309.
[183] G. Wang, Z. Dai, J. Xiao, S. Feng, C. Weng, L. Liu, Z. Xu, R. Huang, Z. Zhang, Bending of multilayer van der Waals materials, Phys. Rev. Lett. 123 (11) (2019) 116101.